

Contents lists available at ScienceDirect

Geoderma

journal homepage: www.elsevier.com/locate/geoderma



Tracing gypsiferous White Sands aerosols in the shallow critical zone in the northern Sacramento Mountains, New Mexico using Sr/Ca and ⁸⁷Sr/⁸⁶Sr ratios



Patrick Rea^a, Lin Ma^a, Thomas E. Gill^a, Jorge Gardea-Torresdey^b, Carlos Tamez^b, Lixin Jin^{a,*}

- ^a Department of Geological Sciences, the University of Texas at El Paso, El Paso, TX 79968, United States
- b Department of Chemistry and Biochemistry, The University of Texas at El Paso, El Paso, TX 79968, United States

ARTICLE INFO

Handling Editor: Alberto Agnelli

Keywords:
Elemental cycles
Dust
Critical zone
Gypsum
Deposition
Nutrient flux

ABSTRACT

White Sands (New Mexico, USA) emits gypsum dust with a unique chemical and mineralogical signature, providing an opportunity to investigate its loading and regional movement. This study tracked White Sands dust input to montane soils downwind in the northern Sacramento Mountains, and provided better understanding of the effects of gypsum dust on sources of bioavailable plant nutrients in an active critical zone. Four soil profiles were collected over bedrocks of different weatherabilities, from the most reactive limestone, mixed limestone, diorite, to the least reactive sandstone, as well as different atmospheric end-members (rain, regional dust, and White Sands gypsum). Annual dry deposition rate observed at the Sacramento Mountains was approximately at 11 g m⁻² yr⁻¹, up to an order of magnitude lower than those at the Chihuahuan Desert basins upwind and closer to dust sources at lower elevations. Elemental chemistry, Ca/Sr and 87Sr/86Sr of bulk soils were mostly controlled by those of bedrocks and modified by chemical weathering over carbonate substrates, whereas the atmospheric input was only detectable in shallow soils over the least reactive sandstone through addition profiles of Ca, Sr and Na. Although only making up a small portion of a bulk soil in mass, White Sands dust, along with wet deposition, dominantly controlled the Ca/Sr and 87Sr/86Sr ratios of plants and the water leachable fraction of the soils. Particles from White Sands, predominantly gypsum, were very soluble, and dissolved quickly in soils of the Sacramento Mountains but re-precipitated at the impermeable bedrock-soil interface. Although absolute concentrations of Ca and Sr in plants differed widely among four sites and among different local plant types, Sr/ Ca ratios were largely controlled by plant type, and thus the rooting depth. This study highlighted the importance of regional dust and rainfall in loading nutrients even in a semi-humid environment.

1. Introduction

In the critical zone, spanning from the top of the trees to the bottom of the groundwater, interactions of rock, soil, water, biota, and the atmosphere occur to support essential ecosystem functions and services (e.g., Brantley et al., 2007; Tchakerian and Pease, 2015). The soil composition of the critical zone varies with bedrock, vegetation cover, and climate, through rates and types of chemical weathering reactions, biological processes, and externally by atmospheric inputs such as rainfall and dustfall (Swap et al., 1992; Reynolds et al., 2006; Derry and Chadwick, 2007; Brantley et al., 2007; Jin et al., 2010; Field et al., 2010; Rasmussen et al., 2011; Lawrence et al., 2013). Dust is dominantly produced in drylands that cover 35% of the Earth's land surface, and transported globally, significantly affecting nutrient cycling (Knippertz and Stuut, 2014; Kumar et al., 2014). Dust is particularly

important in semi-arid ecosystems (Waterfall, 1946; Capo and Chadwick 1999; Reheis et al., 2002; Ewing et al., 2006; Lybrand and Rasmussen, 2018) and also in tropical rainforests with extremely weathered soils where elemental loadings from long-distance transport of dust are detectable (Swap et al., 1992; Pett-Ridge et al., 2009a,b; Bristow et al., 2010; Muhs et al., 2012; Pelt et al., 2013; Kumar et al., 2014). For example, the critical zone nutrient budget in the Amazon Basin has been shown to be affected by dust and biomass burning aerosols from the Saharan Desert (Reynolds et al., 2001, 2006; Abouchami et al., 2013; Barkley et al., 2019). Other instances of aerosol input contributing to elemental additions in soil profiles include dust from the Mojave reaching the Colorado Plateau (Lawrence et al., 2013) and the Channel Islands (Muhs et al., 2008), Saharan aerosol influence in the Andes mountains (Boy and Wilcke, 2008), the European Alps (de Angelis and Guidichet, 1991) and Caribbean and Atlantic islands (Muhs

^{*} Corresponding author at: 500 W. University Ave, El Paso, TX 79968, United States. *E-mail address*: ljin2@utep.edu (L. Jin).

et al., 2007, 2012), Asian and regional dust influence on nutrient cycles in the Sierra Nevada of California (Aciego et al., 2017; Arvin et al., 2017; Aarons et al., 2019) and Hawaii islands (Chadwick et al., 1999), and the Great Basin dusts in western United States influencing surrounding mountain soils (Hoidale and Smith, 1968; Marchand, 1970; Gill. 1996).

However, dust inputs to an ecosystem are commonly difficult to quantify because they generally come from multiple indistinguishable non-point sources involving both short and long-distance transport processes (Derry and Chadwick, 2007; Aciego et al., 2017). As dusts move further downwind, they become mixed and mirror global or regional compositions (Trapp et al., 2010; Bozlaker et al., 2013). In addition, deposition rates and dust chemistry can be spatially and temporally heterogeneous on small and regional scales (Lawrence and Neff, 2009; Perez and Gill, 2009; Huneeus et al., 2011; Hahnenberger and Nicoll, 2012; Vincent et al., 2016; Jiao et al., 2018). To model transport, deposition and fate of dusts, end members of regional dust and local soils must be identified and characterized using unique chemical or isotopic signatures (e.g., Reheis et al., 2002, 2009; Pelt et al., 2013; Arendt et al., 2015; Arvin et al., 2017).

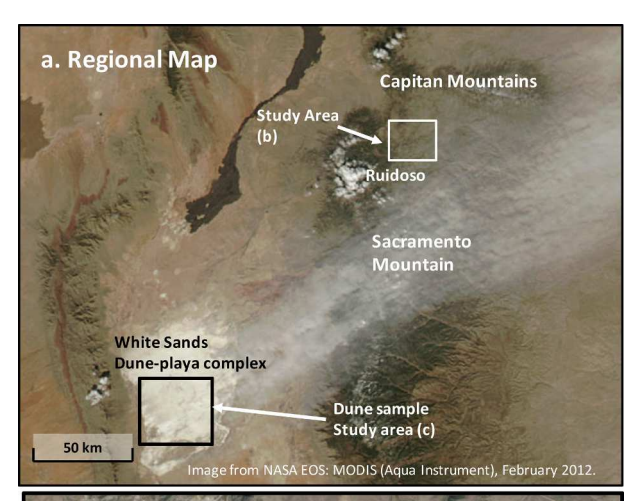
In the Tularosa Basin of New Mexico, the gypsiferous sands from the White Sands National Monument produce visible, intense, and frequent dust plumes that are mineralogically, chemically and maybe even isotopically distinguishable from other local and regional sources of aerosols (Fig. 1A; White et al., 2015; Baddock et al., 2011; Baddock et al., 2016). The prevailing winds from the southwest transport the dust to the east and northeast into the Sacramento Mountains and Sierra Blanca (White Mountain), New Mexico, USA (Fryberger 2001; White et al., 2015), where sufficient precipitation is received annually to make its soils hydrologically and biologically active. These unique conditions make the White Sands – Sacramento Mountains – Sierra Blanca region in New Mexico an ideal place to evaluate if regular emission of White Sands dust makes its signal detectable in soils, investigate its mobility in an active critical zone, and whether White Sands dust becomes an important Ca nutrient source.

Strontium substitutes for calcium in Ca-bearing minerals, and thus elemental ratios (Ca/Sr) and Sr isotopic ratios (87Sr/86Sr) are powerful proxies to identify the sources of base cation Ca and were used here to evaluate elemental fluxes from different sources (Huntington et al., 2000; Dasch et al., 2006; Pett-Ridge et al., 2009b; Jin et al., 2012). In addition, the Sr isotopes are so heavy that the isotope fractionation is typically small through Earth surface processes during biogeochemical cycles such as mineral dissolution, precipitation or biological uptake (Galy et al., 1999; Jacobson and Blum, 2000; Pett-Ridge et al., 2009a,b; Burger and Lichtscheidl, 2019). For this study, elemental ratios (Ca/Sr) and Sr isotopes are combined to identify Ca sources.

Specifically, this work characterized different forms of atmospheric deposition, identified the relative contribution from White Sands dust, and examined the interaction of dust with water and vegetation in an active critical zone in the far northern Sacramento Mountains. Atmospheric versus bedrock inputs on the genesis and evolution of bulk soils were evaluated on four bedrock types (limestone, mixed limestone, diorite, and sandstone). In addition, the mobility of gypsum dust within the soil profiles was investigated by characterizing water leachable components of soils and identified calcium sources in plants.

2. Study areas

The White Sands within the White Sands National Monument of New Mexico, USA are comprised of a series of dunes, interdunes and playas representing the remnants of Pleistocene Lake Otero (Allmendinger and Titus, 1973; Fryberger 2001; Fig. 1). The gypsum dunes are derived from aeolian deflation and transport of evaporitic sands, with new sands derived largely from the ephemeral Lake Lucero (Allmendinger and Titus, 1973; Langford, 2003; Kocurek et al., 2007; Szynkiewicz et al., 2010; Langford et al., 2016). The gypsum originated





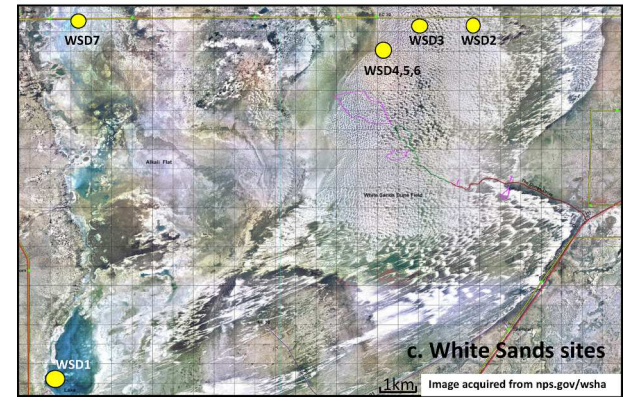


Fig. 1. Regional view of Tularosa basin (a) and study areas within the Sacramento Mountains (b) and the White Sands National Monument (c). Four soil/vegetation sample sites were selected over different lithologies (b). Bedrocks at these four sites have different CaO% contents (labelled next to the site name) and different reactivities. White Sands samples were collected as gypsum dust end members (c).

from the Permian Yeso Formation, which was subsequently exposed, weathered, and accumulated in the Tularosa Basin during the early Holocene (Fryberger, 2001; Kocurek et al., 2007; Langford et al., 2016). The White Sands emit regular and significant plumes of airborne dust northeasterly towards and across Sierra Blanca and the Sacramento Mountains, with variation in dust emission and chemistry controlled by seasonal meteorology and hydrology conditions (White et al., 2015; Fig. 1). The White Sands are a major source of dust in the American Southwest and make the Tularosa Basin and its surrounding ecosystems a natural laboratory for dust studies (Prospero et al., 2002; Rivera Rivera et al., 2010; Baddock et al., 2011; White et al., 2015; Langford

et al., 2016; Baddock et al., 2016).

Uplift and subsidence result in a large relief between the study area at the northern tip of the Sacramento Mountains and the Tularosa Basin (Kelley and Thompson, 1964; Fig. 1a). The peak of Sierra Blanca, to the west of the study area, is 2340 m higher than the Tularosa Basin because of volcanism and Rio Grande rift faulting. This Tertiary volcanism resulted in occurrence of numerous monzonitic laccoliths and stocks, which caused extension and faulting in conjunction with rift faulting in the late Paleozoic and Mesozoic limestones and sandstones in the northernmost Sacramento Mountains (Rawling, 2014). The mean annual temperature at the nearby town of Ruidoso is 10 °C, and the mean annual precipitation is 63 cm (Climate Data 2016, Station RUIDOSO 1.7 WNW, NM US), much cooler and wetter than the neighboring Tularosa Basin (15.2 °C and 27 cm; Capo and Chadwick, 1999). The vegetation types of the study area include Madrean encinal pinyon-juniper woodland, Juniperus monosperma wooded grassland, and semi-desert grasslands (Martin, 1964; Hanks and Dick-Peddie, 1974; Vander Lee et al., 2004).

3. Methods

3.1. Sample collection

Study sites were selected based on slope, aspect, bedrock type, and also to avoid human impacts. Sites facing southwest (primary direction of dust transport) or lying on the top of ridges were chosen because these soils were expected to receive more dust deposition from White Sands than those from east-facing slopes (White et al., 2015). Two (site A and site D) were placed atop ridges; two others (site B and site C) were on steep vegetated slopes and shallow grassy slopes, respectively, facing southwest towards White Sands (Fig. 1b). Sites were selected over bedrock substrates that vary in both composition and mineralogy (Table 1). Lithologies were identified using geologic maps and field observation: site A on Artesia limestone; site B on Champ Hill diorite; site C on San Andres limestone; and site D on Mesa Verde sandstone (New Mexico Bureau of Geology and Mineral Resources, 2003; Rawling, 2014). These soils are mapped by Sprankle (1983) and the USDA Web Soil Survey (websoilsurvey.nrcs.usda.gov) as Aridic Argiustolls (sites A and B), Aridic Calciustolls (site C), and Cumulic Haplustolls (Site D) (Table 1). Sites A, B, and C surround the Sierra Blanca Regional Airport to the northwest, west, and southeast, respectively; site D is 20 km to the northwest near Capitan, New Mexico in the Rio Bonito basin (Fig. 1). A soil pit was dug at each site and soils were sampled at 5 cm intervals on the soil pit wall. If bedrock could not be reached, soils were collected at least to 20 cm deep and rock fragments were collected at the bottom of the soil pits as bedrock. Fresh leaves from most prevalent cacti (Cylindropuntia sp.), grasses (Bouteloua sp.), shrubs (Quercus gambelii, Yucca elata), and trees (the conifers Juniperus monophylla, Pinus edulis) were identified at each site and sampled (Table 1).

To collect dust samples, two vertical falling-dust traps were installed at sites A and C using a USGS protocol (Reheis and Kihl, 1995). A tefloncoated cake pan was filled with marbles and secured to a U-post with chicken wire. The cross-sectional surface area of the pan was 0.14 m². The post was driven into the ground so the traps stayed 1.5 m above ground. The dust pan was checked periodically to prevent overflow from precipitation. The marbles were removed from pans and rinsed with deionized water. The dust sample was recovered after the slurry was left to dry through evaporation in a glass beaker, and weighed. Multiple samples were collected from the field and combined for each site. Dust was collected at site A and site C for 370 days (2/1/2016-9/ 24/2016, and 1/20/2017-6/3/2017) and 302 days (4/9/2016-9/24/ 2016, and 1/20/2017-6/3/2017) respectively. IMPROVE is a national aerosol monitoring network that collects and measures the flux of fine aerosols (PM_{2.5}) at remote sites (Malm et al., 1994; Hand et al., 2011; White et al., 2015; http://vista.cira.colstate.edu/improve/). Data from the IMPROVE WHIT1 site, located near the study sites A, B, and C, were downloaded and analyzed for 11 years (2006-2017).

Surface sediment samples were collected within the White Sands National Monument, in areas more susceptible to erosional loss, dust emission, and subsequent long-range transport (Fig. 1c). Distinct geomorphologies and locations in the White Sands were chosen to constrain potential White Sands end member, recognizing that the episodic dust events might yield a range of White Sands-derived dust signatures (White et al., 2015). Samples were collected from erosional interdunes and dune slip faces with small wind ripples, which are shown to be both fine-grained and sparsely vegetated (Langford et al., 2016). Nine samples were gathered from barchan and parabolic dunes and interdunes, loose sediments below gypsum crusts, as well as flat areas without dunes (Fig. 1; Table 1).

Precipitation chemistry, amount, and annual loading data from the National Atmospheric Deposition Program's National Trends Network (NADP NTN) were downloaded for Mayhill site in Otero County, New Mexico, ~60 km SW of the study sites (2000–2017). To constrain Sr systematics of the regional precipitation, two samples were collected from El Paso, Texas (~190 km SSW of the study sites) in 2018, each covering five months of rain or snowmelt, and analyzed for Sr concentrations by inductively coupled plasma-mass spectrometer (ICP-MS) and Sr isotopes by multi-collector ICP-MS (MC-ICP-MS).

3.2. Sample preparation and analyses

3.2.1. Elemental chemistry, mineralogy and Sr isotope analyses of bulk soil, dust and bedrock samples

Bulk soils were sieved to remove rock fragments that were > 2 mm,

Table 1Characteristics of study sites and various samples.

Site	Latitude (°N)	Longitude (°W)	Soil type	Lithology	Formation	Period/Epoch
Soil profiles:						
Site A	33.472	105.536	Argiustolls	Limestone	Artesia	Permian
Site B	33.461	105.573	Aridic Argiustolls	Diorite	Champ Hill	Oligocene
Site C	33.469	105.515	Aridic Calciustolls	Mixed Limestone	San Andres	Permian
Site D	33.448	105.661	Cumulic Haplustolls	Sandstone/Siltstone	Mesa Verde	Cretaceous
White Sands	samples [†] :					
WS1	32.698	106.451		Selenite/Gypsum		
WS2	32.887	106.123		Gypsum		
WS3	32.886	106.26		Gypsum		
WS4	32.871	106.28		Gypsum, Dolomite		
WS5	32.871	106.271		Gypsum		
WS6	32.871	106.279		Gypsum		
WS7	32.868	106.432		Gypsum		
Dust samples	s: a mixed aggregate of to	tal dust from site A and site	C over 2016–2017			

[†] All White Sands originate from the Permian Yeso Formation, with exposure and onset of dune creation from 11,000 years ago to present.

homogenized and ground down to #100 mesh ($< 150 \mu m$). To prepare for elemental analysis, 100.0 ± 0.5 mg of ground dust, soil, or bedrock samples were weighed, mixed with 1.00 g lithium metaborate, and digested in a furnace at 950 °C for 10 min using methods developed by Feldman (1983). After completely molten, the samples were re-dissolved in 5% HNO3, diluted 1:10 with 5% HNO3, and measured on a Perkin Elmer 5300DV inductively coupled plasma optical emission spectrometer (ICP-OES) for concentrations of major elements and Sr. Rock standards (n = 24) were similarly digested and prepared, and used for calibration. Duplicates were run to measure precision, and two procedure blanks were run for quality control and assurance. Concentrations between duplicates varied by < 5%, except for SiO₂, so SiO₂ data were not reported or discussed further. For Sr. analytical precisions were lower than those of major elements, as up to 11% difference (average 3%) was observed in Sr concentrations between duplicates. Procedure blank for the lithium metaborate fusion method was low, < 1 wt% for sum of all major oxides and 18 ppm for Sr.

Mobile elements or oxides (e.g., CaO, Sr) are conventionally normalized to an immobile element (e.g., Ti or Zr) in order to characterize dynamics of these mobile elements in soil profiles. Mass transfer coefficients τ are calculated according to the following equation (Brimhall and Dietrich, 1987; Anderson et al., 2002; Brantley et al., 2007):

$$\tau_{i,j} = \left(\frac{C_{j,w} C_{i,p}}{C_{j,p} C_{i,w}}\right) - 1$$

where C is the concentration of an immobile (i) or a mobile (j) element in weathered (w) or parent (p) material. Typical τ depth profiles indicate unique geochemical behaviors for a given mobile element j: an immobile profile if $\tau=0$, depleted by leaching if $\tau<0$, enriched if $\tau>0$, translocated if $\tau<0$ at surface but $\tau>0$ at depth, or a biogenic profile if $\tau<0$ at depth but $\tau>0$ at surface) (Brantley et al., 2007). For this study, titanium (Ti) was used as the immobile element, and relative errors were assumed to be 5% in analyzing concentrations of major elements (e.g., Ca, Ti), and 10% in trace elements (Sr). Bedrock heterogeneity was assumed to contribute little to uncertainties in C_p . Error in mass transfer coefficient τ was propagated based on relative uncertainties in $C_{j,w}$ $C_{j,p}$, $C_{j,p}$, and $C_{i,w}$ (Jin et al., 2010).

Major minerals in bedrock and soil samples were identified using X-ray powder diffraction (XRD) and their relative abundance was qualitatively evaluated based on peak intensity. Finely ground samples were prepared on a thin section and analyzed on a Rigaku XRD with CuK α , from 10° to 65° (20) at a 0.03° step size and 1.5° /min scan speed. EVA DIFFRAC Suite software was used to identify peaks using the ICDD PDF-2 XRD database (2008 release).

Bulk soil samples were analyzed for total carbon (TC), and total organic carbon (TOC). Approximately 0.25 g of soil was weighed and combusted at 1350 °C with 1.0 g of combustion aid (com-aid) on a LECO SC632 Sulfur/Carbon determinator. Two standards of different C concentrations (LECO 502-062 and LECO 502-814) were used for calibration and check standards. Total organic carbon was quantified after carbonates were removed with 1:1 HCl solution and samples were dried in the oven at 60 °C. The difference between total carbon and total organic carbon was attributed to inorganic carbon, or carbon in carbonate minerals. Check standards were measured within < 1% relative error of the certified values and duplicate samples agreed with each other within 5%. Not enough dust sample was available for C analysis; instead, loss on ignition (LOI) was performed on dust samples at 550 °C to estimate organic matter contents.

For Sr isotope analysis, 100 mg of ground soil or rock samples were weighed, put into clean Teflon beakers, and digested using concentrated hydrofluoric and nitric acids. Solutions were evaporated, redigested with boric and hydrochloric acid, evaporated again, and redissolved in 3.5 N nitric acid (Pett-Ridge et al., 2009a,b). Sample purification was conducted through column chemistry and isotope ratio measurement was conducted on a MC-ICP-MS, as described below.

3.2.2. Water leachates of soil, White Sands, and dust samples: Elemental chemistry and Sr isotopes

The water-soluble fraction of soil or dust isolated any evaporite salts, including gypsum. A solid sample (soil, dust, White Sands) was weighed with a set volume of deionized water, mixed into a slurry via hand shaking for about one minute, and then centrifuged at 3500 rpm for 10 min. The supernatant solution was filtered through a 0.45 μm cellulose acetate syringe filter, and then analyzed for major element concentrations, and electrical conductivity (EC) and pH using calibrated electrodes and hand meters. For cation concentrations, leachate samples were diluted with deionized water and then acidified using 3 drops of concentrated nitric acid before ICP-OES analysis. USGS reference standards M178, M182, and M210 were run as checks for quality control. Duplicate solution samples and procedure blank were run for quality assurance. Leachates were diluted with deionized water before ion chromatograph (IC, Dionex ICS-2100) analysis for anion concentrations. A check standard was made by diluting Alltech anion mix standard A and run along with unknown samples, a procedure blank and duplicates. The concentrations of Ca2+ and Sr2+ in check standards were measured within the certified values by 3.4% and 3.5%, respectively. Check standards were measured within 10% of reference values for all anions (2% for F⁻, 9% for Cl⁻, 4% for SO₄²⁻, 2% for $\mathrm{NO_{3.}^{-}}$ and 6% for $\mathrm{PO_{4}^{3-}}$). For Sr isotope analysis, sample purification was conducted through column chemistry and isotope ratio measurement was conducted on a MC-ICP-MS, as described below.

3.2.3. Major element chemistry and Sr isotopes of plants

Plant leaves were rinsed with deionized water to remove surface dust, oven dried, ground and homogenized. Samples were then digested following EPA method 3050B. Specifically, 0.20 g of a ground leaf sample was weighed, mixed with 5 mL concentrated nitric acid, placed in a hot digestion block, and then diluted to 50 mL with deionized water to a 5% nitric acid solution. The diluted solution was measured on the ICP-OES for concentrations of major and minor elements.

To prepare for Sr isotopes, vegetation samples were put into Teflon Parr bomb digestion containers with 6 mL of concentrated nitric acid. Pressure built up for 24 h at 100 °C, and after cooling, samples were collected and evaporated. Dried samples were re-dissolved in 3.5 N $\rm HNO_3$ and centrifuged, and 1 mL of sample was used for column chemistry.

3.2.4. Sr isotope analysis by MC-ICP-MS

Strontium isotope ratios (87Sr/86Sr) of rainwater, and leachates of soil/dust and digestions of dust, soil, rock, and plant samples were run on the Nu plasma HR MC-ICP-MS at The University of Texas at El Paso after elution of extraneous elements through a column chemistry procedure (Konter and Storm, 2014). The prepared samples were run through a column filled with Eichrom Sr-resin to extract and purify strontium; other elements were eluted out in a series of 3.5 N nitric acid aliquots until the Sr is collected using 0.05 N nitric acid. This procedure was done twice for each sample (only once for plants), and between runs a sample solution was evaporated and re-dissolved in 3.5 N nitric acid. A procedure blank was run for each batch of samples to identify potential background contamination. The procedure blank for Sr was negligible. Standard SRM-987 was used for sample bracketing for instrument drift and run after each set of 3 samples. Check standard BCR-2 was run with samples repetitively as well, with an average of 0.70500 ± 0.00002 (n = 4), within the certified value of $0.70502 \pm 0.00001.$

4. Results

4.1. Bulk soil/dust/rock mineralogy, elemental chemistry, and Sr isotopes

XRD spectra and major minerals identified were shown for bedrock and representative soil samples from these four study sites (Appendix

Table 2
Elemental chemistry and Sr isotope ratios of bulk soil and bedrock samples from Sacramento Mountains region, NM.

Soil profile	Depth cm	Al ₂ O ₃ %	CaO %	Fe ₂ O _{3(T)} %	K ₂ O %	MgO %	MnO %	Na ₂ O %	P ₂ O ₅ %	$^{\rm TiO_2}_{\%}$	Ba ppm	Sr ppm	Zr ppm	Ca/Sr mol/mmol	TC %	TOC %	calcite*	⁸⁷ Sr/ ⁸⁶ Sr
A00	0–5	14.2	5.7	4.26	3.16	1.25	0.08	2.12	0.23	0.77	866	272	281	0.32	4.0	3.7	2.8	0.7080
A05	5-10	13.2	6.3	4.05	2.80	1.16	0.07	1.79	0.13	0.72	782	275	342	0.36	3.9	3.2	5.6	0.7088
A10	10-15	13.8	7.2	4.21	2.89	1.22	0.07	1.93	0.20	0.75	848	276	308	0.41	3.9	3.1	6.4	0.7077
A15	15-20	14.1	8.2	4.35	3.02	1.26	0.08	1.94	0.17	0.77	878	295	281	0.43	3.7	3.0	6.2	0.7087
A20	20-25	13.5	7.3	4.14	2.86	1.17	0.07	1.79	0.17	0.74	815	284	352	0.40	3.7	2.8	7.3	0.7087
A25	25-30	14.0	9.9	4.18	3.06	1.18	0.07	2.08	0.22	0.74	885	295	331	0.52	4.0	2.8	9.9	0.7087
A30	30-35	13.4	14.0	3.91	2.96	1.09	0.06	1.91	0.23	0.71	822	303	345	0.72	4.8	2.9	15.4	0.7086
A35	35-40	14.4	24.0	4.68	3.82	1.35	0.08	2.46	0.33	0.84	1743	466	379	0.80	5.6	2.8	23.0	0.7084
A40	40-50	11.5	21.3	3.35	2.46	1.02	0.05	1.59	0.22	0.58	747	319	260	1.04	5.9	2.4	29.4	0.7084
A50	50-60	9.2	31.4	2.53	2.01	0.86	0.04	1.51	0.16	0.45	927	373	175	1.32	7.5	1.8	48.0	0.7079
A:bedrock	65	2.9	51.4	0.71	0.50	0.52	0.01	0.26	0.11	0.10	369	301	94	2.67	11.7	0.5	93.0	0.7083
B00	0–5	16.4	2.3	6.04	4.43	1.20	0.14	3.17	0.21	1.16	1703	422	473	0.08	4.0	4.3	BDL	0.7080
B05	5-10	16.4	2.5	5.23	3.56	1.14	0.11	2.48	0.15	0.95	903	321	382	0.12	3.4	3.2	BDL	0.7077
B10	10-15	16.4	2.0	5.18	3.56	1.09	0.09	2.57	0.07	0.92	915	322	338	0.10	2.5	2.5	BDL	0.7089
B15	15-20	17.1	2.3	5.31	3.72	1.20	0.09	2.66	0.13	0.95	950	330	401	0.11	2.4	2.4	BDL	0.7075
B20	20-35	17.0	1.9	5.20	3.62	1.13	0.09	2.63	0.09	0.94	889	310	278	0.10	2.0	2.2	BDL	0.7073
B35	35-40	18.3	2.5	5.62	3.87	1.31	0.10	2.82	0.07	0.95	1041	348	371	0.11	1.9	1.9	BDL	0.7070
B:bedrock	45	16.3	2.1	4.32	4.32	0.75	0.13	3.60	0.22	0.84	1104	238	486	0.14	1.5	1.6	BDL	0.7072
C00	0–5	15.0	7.6	4.94	3.20	1.28	0.09	2.43	0.26	0.85	892	351	329	0.34	3.4	2.5	7.4	0.7075
C05	5-10	14.1	6.2	5.03	2.83	1.36	0.09	2.00	0.24	0.86	781	326	354	0.30	3.7	3.1	4.7	0.7073
C10	10-15	14.2	8.1	5.02	2.90	1.28	0.08	2.15	0.24	0.85	821	338	342	0.38	3.1	2.0	9.4	0.7078
C15	15-20	13.4	6.5	4.64	2.68	1.24	0.08	2.04	0.19	0.77	762	305	293	0.33	3.4	2.6	6.4	0.7074
C20	20-25	14.4	7.5	5.04	2.90	1.32	0.09	2.14	0.23	0.88	819	332	359	0.35	3.2	2.2	8.0	0.7074
C25	25-30	14.1	7.9	4.84	2.89	1.27	0.08	2.14	0.18	0.83	807	326	336	0.38	3.1	2.0	8.6	0.7074
C30	30-35	14.1	8.3	4.80	2.82	1.26	0.08	2.10	0.17	0.82	814	335	396	0.39	3.1	1.9	9.7	0.7075
C35	35-40	12.7	8.7	4.69	4.42	1.24	0.08	3.30	0.49	0.79	782	353	302	0.38	2.8	1.6	10.2	0.7074
C40	40-45	13.0	9.5	4.94	2.87	1.26	0.08	2.03	0.21	0.83	817	365	377	0.41	3.0	1.6	11.8	0.7076
C45	45-50	13.8	9.4	4.80	2.82	1.23	0.08	2.00	0.20	0.84	803	352	308	0.42	3.3	1.8	12.0	0.7075
C:bedrock	55	14.2	8.6	3.95	3.49	0.91	0.08	2.44	0.27	0.73	784	262	475	0.51	2.7	0.1	21.9	0.7100
D00	0–5	9.3	0.9	3.55	1.47	0.62	0.05	1.41	0.12	0.58	454	225	350	0.06	1.0	n.d.	n.d.	0.7103
D05	5-10	10.2	1.0	3.90	1.70	0.73	0.05	1.38	0.20	0.67	459	222	391	0.07	1.2	n.d.	n.d.	0.7108
D10	10-15	12.2	0.8	4.50	1.67	0.84	0.05	0.73	0.07	0.65	449	160	340	0.08	1.4	n.d.	n.d.	0.7107
D15	15-20	18.8	1.3	6.83	2.48	1.24	0.08	1.32	0.28	0.97	720	242	469	0.09	1.3	n.d.	n.d.	0.7112
D20	20-25	12.5	0.9	4.69	1.74	0.88	0.05	0.83	0.10	0.66	589	174	379	0.08	1.3	n.d.	n.d.	0.7112
D:bedrock	30	7.7	0.2	7.06	0.56	0.94	0.02	0.75	0.04	0.62	1227	101	562	0.03	0.2	n.d.	n.d.	0.7108
Dust	n.d.	n.d.	n.d.	n.d.	n.d.	n.d.	n.d.	n.d.	n.d.	n.d.	n.d.	n.d.	n.d.	n.d.	n.d.	36.4	n.d.	0.7087

n.d. = not determined; BDL = below detection limit.

Fig. 1). Site A showed nearly pure calcite in bedrock, and quartz and microcline peaks became more pronounced relative to that of calcite in soil samples towards surface. The bedrock contained predominantly quartz, plagioclase, and microcline at site B, and similar mineralogy was observed in soils. The bedrock was comprised of calcite, quartz, feldspars, and hornblende at site C, and quartz and calcite increased in relative abundance towards soil surface. The bedrock and soils at site D were dominated by quartz with minor microcline. All White Sands dune samples were comprised almost completely of gypsum; Lake Lucero sediments showed traces of halite and mirabilite (Na₂SO₄·10H₂O); Bulk dust from sites A and C contained mainly quartz, calcite, plagioclase and microcline with no detectable gypsum (Appendix Fig. 1).

All elemental and isotopic data for bulk soil and rock samples were reported in Table 2. The CaO contents in bulk soils increased sharply with depth at site A (from 5.7 to 31.4 wt%), and at site C (from 7.6 to 21.8 wt%), but remained low and relatively unchanged with depth at site B (from 2.0 to 2.5 wt%) and at site D (from 0.8 to 1.3 wt%). Other elements (Fe, Al, K, and Na), dominant in silicate minerals, decreased in their abundance with depth at sites A and C. For instance, Al₂O₃ content decreased from 14.2 to 9.2 wt%, and from 15.0 to 12.7 wt% at site A and site C, respectively. In contrast, the Al₂O₃ content in bulk soils increased slightly with depth at site B (16.4 to 18.3 wt%) and at site D (9.3 to 12.5 wt%). The MgO content remained relatively constant at site A (0.9 to 1.2 wt%), site B (1.1 to 1.3 wt%), and site C (1.1 to 1.3 wt%), and increased slightly with depth at site D (0.6 to 1.3 wt%). Depth trends of bulk soil Sr contents followed those of CaO in all four profiles.

However, the Ca/Sr ratios increased with depth in all four soil profiles and reached those of the bedrock at the soil-bedrock interface (Table 2; Fig. 2B): 0.32 to 1.32 mol/mmol at site A, 0.08 to 0.11 mol/mmol at site B, 0.34 to 0.42 mol/mmol at site C, and 0.06 to 0.09 mol/mmol at site D.

Contents of total organic carbon (TOC) in soils decreased with depth in all four soil profiles (Table 2). Contents of inorganic carbon (difference between total carbon and total organic carbon) increased with depth at site A and site C, over carbonate bedrock. Inorganic carbon content was stoichiometrically converted to calcite wt% based on minerals identified via XRD (Table 2). Site A, developed on limestone, had a sharp increase of calcite contents in soils below 25 cm (up to 48 wt% calcite), and site C, developed on mixed limestone, had up to 12 wt% calcite in soils. Up to 61% of total CaO measured at site A and up to 20% at site C were attributed to carbonates while the rest in silicate minerals such as plagioclase (Table 2). Inorganic carbon contents were mostly not detectable in soil and bedrock samples at site B and site D.

Within the large uncertainty in mass transfer coefficient τ , CaO showed a depletion profile at site A, was slightly depleted in sites B and C relative to bedrock, but was greatly enriched at site D ($\tau > 3$) (Appendix Fig. 2). Similarly, Sr was depleted at site A, almost immobile at sites B and C, and enriched at site D (0.25 < $\tau < 1.8$). MgO was depleted at sites A and D, and slightly enriched at sites B and C. Na₂O is immobile at site A, depleted at sites B and C (apart from 35 to 40 cm,) and added at site D.

The 87Sr/86Sr ratios in bulk soils varied between 0.7070 and 0.7089

^{*} Calcite % was estimated by soil inorganic carbon concentrations and CaCO3 stoichiometry, difference in total carbon (TC) and total organic carbon (TOC).

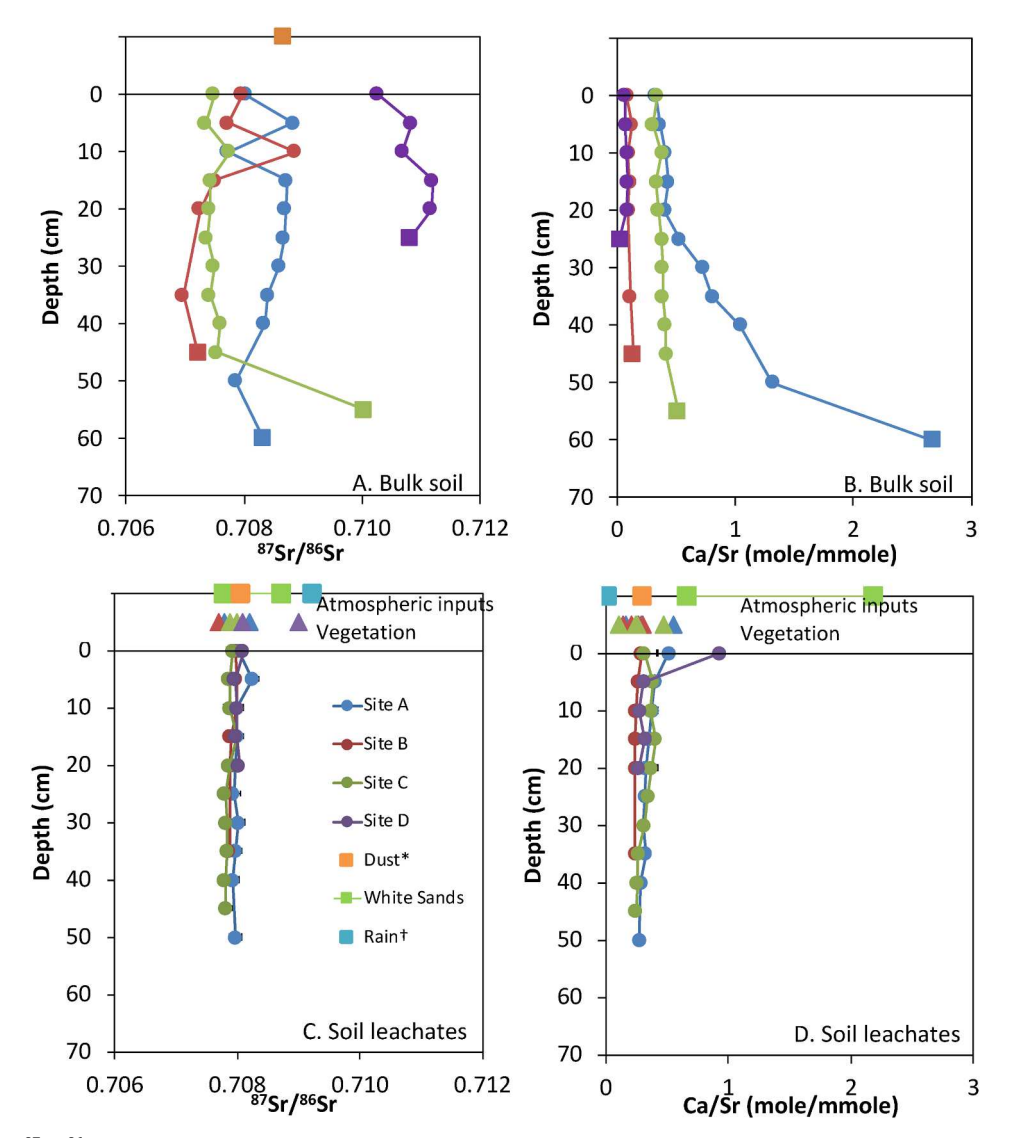


Fig. 2. Depth profiles of 87 Sr/ 86 Sr (A) and Ca/Sr (B) in bulk solid samples (soils in circles, underlying bedrock in squares, dust samples placed at -10 cm) and of 87 Sr/ 86 Sr (C) and Ca/Sr (D) in soil leachates and vegetation samples (triangles, placed at -5cm) at four sites. The plant samples are grouped based on sites. *Dust leachate contains some rain water. † Ca/Sr and 87 Sr/ 86 Sr ratios plotted for rain samples from El Paso, Texas.

at sites A, B, and C, but were much higher at site D (0.7103 to 0.7112) (Table 2; Fig. 2A). The strontium isotope ratios were variable for the top 15 cm soils at site A, and decreased steadily from 0.7087 to 0.7079 in soils from 15 to 50 cm depth, with the ⁸⁷Sr/⁸⁶Sr ratio of limestone bedrock measured at 0.7083. The ⁸⁷Sr/⁸⁶Sr ratios in bulk soils at Site B generally decreased with depth from 0.7075 to 0.7070 with more variability at top 15 cm, and the diorite bedrock had the ⁸⁷Sr/⁸⁶Sr ratio of 0.7072. At site C, the Sr isotope ratios in bulk soils varied little between 0.7074 and 0.7076, different from the bedrock at 0.7100. The ⁸⁷Sr/⁸⁶Sr ratios at site D increased in bulk soils with depth from 0.7103 to 0.7112, with a bedrock ratio of 0.7108.

4.2. Elemental and Sr isotope data for soil and dust samples: water-soluble fraction

Concentrations of major elements, Ca/Sr molar ratios, Sr isotopes, pH and EC data for water-leachable fraction of each soil were reported in Table 3. Soil pH varied between 6.7 and 7.2 over the limestone substrate at site A, and 6.7 to 7.5 at site C. Soils at site B, developed over Tertiary diorite, had slightly lower pH than those at site A, ranging from 6.0 to 7.0. Soil pH at site D over sandstone, was the lowest from 6.1 to 6.5. The soil to water ratios in the soil leaching procedure were

different among soils from four sites, from 302 to 352 g soil per liter of water at sites A, B and C. Thus, measured EC values in the water leachates cannot be directly compared. Even so, the EC of the soil leachates were lower at site B, from 56 to 117 $\mu s/cm$, than those at site A and site C, from 98 to 197 $\mu s/cm$. Also, the EC increased gradually with depth. Limited by sample availability, less soils were used for leaching at site D (130 to 145 g soil per liter of water), leading to lower EC (28 to 41 $\mu s/cm$). With 34.8 g dust per liter of water, the EC of dust leachate was much higher than soil EC, at 47.2 mS/cm (47200 $\mu S/cm$). The highest EC values were observed on White Sands leachates, even with extremely low solid to water ratio (0.5 to 1.1 g per liter of water).

The dominant cations in soil leachates were ${\rm Ca}^{2+}$ and ${\rm K}^+$, and the dominant anions were ${\rm SO_4}^{2-}$ and ${\rm Cl}^-$, with detectable ${\rm NO_3}^-$ and ${\rm PO_4}^{3-}$ at some of the surface soils (Table 3). Water-soluble ${\rm Ca}^{2+}$ in soils followed the same trend as EC, highest at site D, and lowest at site B (Fig. 3A). Water soluble ${\rm SO_4}^{2-}$ in soils increased strongly with depth at each site, with the highest concentrations also observed at site D (Fig. 3B). The Ca/Sr molar ratios in water-soluble fraction of soils decreased with depth at all sites from 0.93 to 0.24 mol/mmol (Fig. 2D). A relatively higher Ca/Sr ratio was observed from the surface soil in all sites, with a mean 0.5 \pm 0.3 mol/mmol. The $^{87}{\rm Sr}/^{86}{\rm Sr}$ in soil leachates varied little among sites or with depth between 0.7078 and 0.7083

Sample	pН	EC μS/cm	Soil:Water g/L	Al mg/kg	Ca mg/kg	K mg/kg	Mg mg/kg	Na mg/kg	Si mg/kg	Sr μg/kg	F mg/kg	Cl mg/kg	SO ₄ μg/kg	NO ₄ mg/kg	PO ₄ mg/kg	⁸⁷ Sr/ ⁸⁶ Sr	Ca/Sr mol/mmol
A00	7.2	107	345	0.3	21.9	2.4	1.2	BDL	6	93	1.3	2.0	3.3	26.1	2.1	0.7080	0.51
A05	7.0	98	334	0.2	22.4	0.8	1.4	1	2	123	2.5	1.9	6.5	9	0.9	0.7083	0.40
A10	7.0	106	339	0.3	19.2	0.6	1.2	1	2	113	2.6	2.0	6.5	11	1.1	0.7080	0.37
A15	7.2	128	351	0.2	25.0	1.6	1.7	4	2	156	4.7	2.4	18.7	8	1.0	0.7080	0.35
A20	6.7	172	321	0.2	24.8	2.0	1.8	3.6	2.2	166	4.4	1.7	13.6	1	1.1	0.7080	0.33
A25	6.8	141	351	0.2	27.1	2.1	2.0	4.4	2.0	186	4.5	1.7	23.0	1.9	0.6	0.7079	0.32
A30	7.2	133	347	0.2	23.7	2.9	1.8	3.9	1.7	170	5.2	1.7	21.7	2	0.5	0.7080	0.31
A35	6.9	156	352	0.2	27.7	2.7	2.2	4.0	1.3	187	3.3	3.5	69.8	4.1	0.9	0.7080	0.32
A40	7.0	127	336	0.2	21.8	3.1	1.7	2.8	1.2	167	4.3	1.8	26.4	3	0.8	0.7079	0.29
A50	7.1	168	302	0.2	35.0	2.6	3.0	6	1	282	3.8	3.9	120.4	3	0.7	0.7080	0.27
B00	6.5	56	334	1.6	10.9	3.5	1.7	0.4	10.1	81	0.6	1.3	4.6	5	8.7	0.7080	0.29
B05	6.5	63	334	2.7	13.2	4.0	2.0	1	13	110	3.8	2.9	10.6	4	2.4	0.7080	0.26
B10	6.0	73	342	2.7	11.6	3.5	1.9	2	12	104	5.1	4.8	27.4	3.2	2.8	0.7080	0.24
B15	6.0	84	341	1.4	14.2	3.0	2.0	3	10	130	3.5	5.3	47.0	6	1.8	0.7079	0.24
B20	6.0	91	338	0.6	14.8	2.9	2.0	4.1	8.1	136	3.4	4.6	64.1	1	1.9	0.7079	0.24
B35	7.0	117	334	0.3	20.4	3.2	2.9	3.9	8.1	185	3.4	3.6	41.3	1	0.8	0.7079	0.24
C00	7.0	173	341	0.2	34.9	5.5	2.3	2.3	5.9	243	2.7	4.2	35.3	62.8	1.1	0.7079	0.31
C05	7.1	130	333	0.2	26.6	3.7	1.6	1	7	153	2.5	8.1	11.4	19.2	1.0	0.7079	0.38
C10	7.4	154	343	0.3	29.7	2.6	1.9	1	6	177	0.7	5.0	15.9	30	0.4	0.7079	0.37
C15	7.3	140	341	0.2	30.3	2.4	1.7	2	5	164	1.0	4.4	18.3	24	0.4	0.7080	0.40
C20	7.1	157	337	0.2	31.8	1.8	1.7	4	3	189	1.3	3.4	37.7	10.8	0.4	0.7079	0.37
C25	7.5	155	341	0.2	32.6	1.8	1.7	3.1	3.0	208	2.0	4.1	29.0	7	0.4	0.7078	0.34
C30	6.7	175	340	0.2	36.4	3.0	2.3	4.2	2.6	255	4.0	2.3	39.7	5	1	0.7078	0.31
C35	7.1	161	333	0.2	35.1	1.6	2.3	4.3	2.6	290	3.4	1.4	31.6	24	0.3	0.7078	0.26
C40	7.3	165	333	0.2	35.2	1.8	2.3	3.8	2.5	302	3.7	1.1	36.7	16	0.3	0.7078	0.25
C45	7.4	197	339	0.2	39.2	2.4	2.9	4.2	2.9	347	4.2	2.3	73.4	4	0.2	0.7078	0.25
D00	6.1	29	138.7	0.4	14.1	2.8	0.4	2.3	2.0	33	0.0	34.0	5.0	41.6		0.7081	0.93
D05	6.4	33	132.7	6.5	46.7	18.4	4.1	14.6	34.6	334	0.3	13.5	31.4	BDL		0.7080	0.31
D10	6.5	28	129.7	6.3	47.7	16.3	4.8	18.6	33.4	386	0.4	18.6	53.2	20		0.7080	0.27
D15	6.5	34	145.3	4.8	58.2	20.4	5.0	22.2	28.7	402	0.4	10.5	64.2	2		0.7080	0.32
D20	6.5	41	144.0	4.4	69.4	21.3	6.4	22.8	32.6	572	0.6	27.9	86.5	BDL		0.7080	0.27
Dust ^T	6.6	47200	34.8	73	9268	6209	345	10428	010	67852	68	20688	15222	1266		0.7081	0.30
WS1	n.d.	1308	1.2	134	213158	210			213	213100	636	2914	451249	12926		0.7087	2.19
WSD2	n.d.	1321	1.1	154	274437	81			821	820890	745	737	508022	12006		0.7078	0.73
WSI2	n.d.	610	0.5	n.d.	n.d.	n.d.		n.d.		n.d.	n.d.	n.d.	458589	n.d.		0.7078	
WSD3	n.d.	874	0.7	n.d.	n.d.	n.d.		n.d.		n.d.	n.d.	n.d.	433889	n.d.		0.7078	
WSI3	n.d.	578	0.5	n.d.	n.d.	n.d.		n.d.		n.d.	n.d.	n.d.	354939	n.d.		0.7078	
WSD4	n.d.	575	0.5	n.d.	n.d.	n.d.		n.d.		n.d.	n.d.	n.d.	580944	n.d.		0.7078	
WSD4d	n.d.	608	0.5	n.d.	n.d.	n.d.		n.d.		n.d.	n.d.	n.d.	525214	n.d.		0.7079	
WSD5	n.d.	653	0.6	n.d.	n.d.	n.d.		n.d.		n.d.	n.d.	n.d.	463080	n.d.		0.7078	
WSD6	n.d. n.d.	722	0.6	n.d.	n.d.	n.d.		n.d.		n.d.	n.d.	n.d.	461608	n.d.		0.7079	
WSD7	n.a.	603	0.6	n.d.	n.d.	n.d.		n.d.		n.d.	n.d.	n.d.	482951	n.d.		0.7079	

^{*}Gypsum content was estimated based on sulfate concentrations and CaSO₄ stoichiometry.

[†] Dust samples contained rain water and snowmelt.

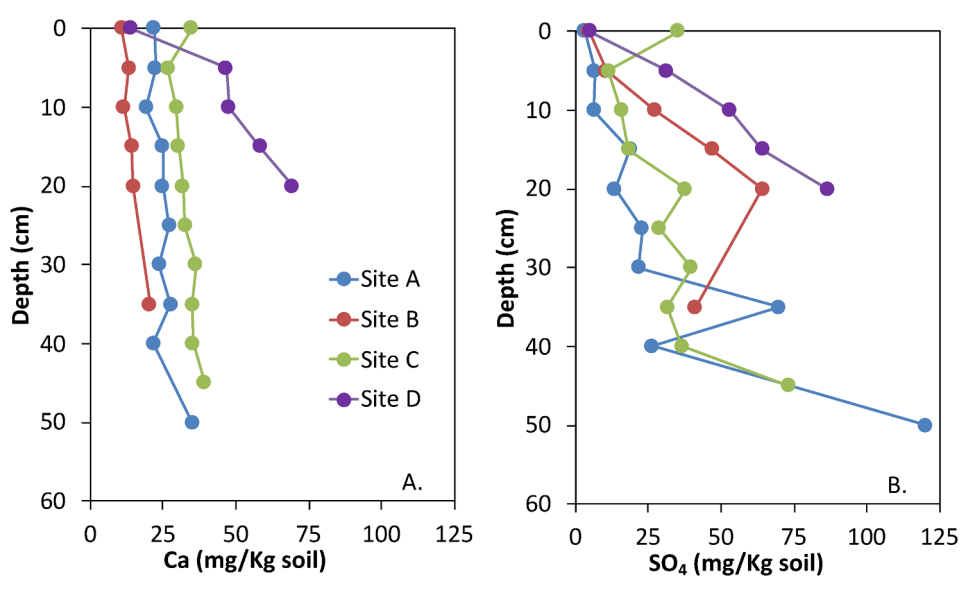


Fig. 3. Depth profiles of calcium concentration (A) and sulfate concentration (B) in water soluble fraction of soil samples at four sites.

n.d. = not determined BDL = below the detection limit.

(average at 0.7079 \pm 0.0001; n = 30; Fig. 2C).

Only 6.4 wt% of the bulk dust was water soluble, dominated by dissolved ${\rm Ca^{2}}^+$ (9 g/kg dust), ${\rm Na^+}$ (10 g/kg dust), ${\rm K^+}$ (6 g/kg dust), ${\rm Cl^-}$ (21 g/kg dust) and ${\rm SO_4}^{2-}$ (15 g/kg dust) (Table 3). In addition, trace amounts of water-soluble Al, Fe, Mg, Mn, and F were detected with concentrations below 1 g/kg dust. The Ca/Sr ratio was 0.30 mol/mmol, ${\rm SO_4}^{2-}/{\rm Ca^{2+}}$ molar ratio was 0.56, and the ${\rm ^{87}Sr/^{86}Sr}$ ratio of water leachable fraction of dust was 0.7081.

The White Sands samples dissolved completely in water, although only ${\rm SO_4}^{2-}$ concentrations were measured (Table 3). The ${\rm SO_4}^{2-}/{\rm Ca}^{2+}$ ratios were assumed to be 1 in the following discussion for White Sands end-member although these measurements were slightly different from 1 due to presence of phases other than pure gypsum. The water leachable Ca/Sr ratio was 0.66 mol/mmol in White Sands dune samples, and 2.2 mol/mmol in the Lake Lucero sediment. The Sr isotope ratios in leachates of the White Sands samples had a narrow range between 0.7078 and 0.7079, except for Lake Lucero sediments (0.7087) (Table 3).

4.3. Elemental and Sr isotope data for plant samples

Plant chemistry data including Sr isotopes were reported in Table 4. Total concentrations for elements that were measured in dried plant biomass (Al, Ca, Fe, K, Mg, Mn, Na, and Sr) ranged from 1.6 ± 0.4 wt % at site A, 2.8 ± 1.4 wt% at site B, and 4.8 ± 2.5 wt% at site C (not measured at site D). Dominant elements in all plants from all sites were Ca (mean: 1.1 wt%), K (mean: 0.6 wt%), and Mg (mean: 0.2 wt%). However, Na was only measurable in plants of site C (mean: 2.4 wt%). Interestingly, Ca concentrations varied more between specific plant types than between sites: 0.26-0.52 wt% in grasses, 0.7-1.5 wt% in conifers and shrubs, 3.2 wt% in cactus from site B. Site B had sum of these elements at 1.2 ± 0.5 wt%, significantly higher than both site A (mean 0.6 ± 0.2 wt%) and site C (mean 0.3 ± 0.2 wt%). This may be due to the extensive vegetation cover over site B by conifers that trapped falling dust above the soil surface (Farmer, 1993), while sites A and C were more chemically similar over more grassy areas.

The Ca/Sr ratios ranged from 0.21–0.29 in grasses, 0.10–0.30 in conifers, 0.25–0.55 in shrubs, and was 0.27 in the cactus at site B (Fig. 2D). Among all sites, shrubs had the highest Ca/Sr ratios, followed by grasses, and then conifers. *Juniperus monosperma* from site B was the exception with a relatively high Ca/Sr ratio of 0.3 mol/mmol, significantly different from other conifers. The Sr isotope ratios of plants samples had a quite narrow range (Table 4; Fig. 2C; grasses: 0.7082, 0.7079, 0.7080, and 0.7090; shrubs: 0.7078, 0.7077, 0.7080, and 0.7081; conifers: 0.7077, 0.7077, 0.7079, and 0.7081).

 Table 4

 Elemental chemistry and Sr isotope ratios of plant samples.

Sample	Genus/species	ID	Al ppm	Ca ppm	Fe ppm	K ppm	Mg ppm	Mn ppm	Sr ppm	Ca/Sr mol/mmol	⁸⁷ Sr/ ⁸⁶ Sr
Site A: Grass	Bouteloua sp	AG	1143	3436	1278	2597	710	68	26	0.29	0.7082
Site A: Conifer	Pinus edulis	AP	78	8632	78	5290	997	21	120	0.16	0.7077
Site A: Shrub	Quercus gambelii	AS	62	11,246	68	6634	1352	260	45	0.55	0.7078
Site B: Cactus	Cylindropuntia sp	BC	31	32,320	24	11,542	7733	70	262	0.27	0.7077
Site B: Grass	Bouteloua sp	BG	1331	5222	1408	5740	1086	85	56	0.21	0.7079
Site B: Conifer 1	Juniperus monosperma	BP1	98	9348	98	11,385	2604	121	67	0.30	0.7077
Site B: Conifer 2	Juniperus monosperma	BP2	85	14,491	88	4800	1281	38	229	0.14	0.7077
Site B: Shrub	Quercus gambelii	BS	97	10,950	114	10,015	1539	321	80	0.30	0.7077
Site C: Grass	Bouteloua sp	CG	118	2619	112	653	225	31	24	0.24	0.7080
Site C: Conifer	Juniperus monosperma	CP	115	6689	80	4293	945	14	139	0.10	0.7079
Site C: Shrub 1	Quercus gambelii	CS1	99	14,512	71	2470	1402	74	68	0.47	0.7080
Site C: Shrub 2	Yucca elata	CS2	47	6660	38	8453	937	94	58	0.25	0.7080
Site D: Grass	Bouteloua sp	DG	n.d.	n.d.	n.d.	n.d.	n.d.	n.d.	n.d.	n.d.	0.7090
Site D: Conifer	Juniperus monosperma	DP	n.d.	n.d.	n.d.	n.d.	n.d.	n.d.	n.d.	n.d.	0.7081
Site D: Shrub	Artemesia filifolia	DS	n.d.	n.d.	n.d.	n.d.	n.d.	n.d.	n.d.	n.d.	0.7081

n.d. = not determined.

4.4. Elemental concentrations and fluxes through rain and dust

The annual precipitation and elemental loading data, downloaded from NADP, were reported in Appendix Table 1. The amount of annual rainfall for the study region varied dramatically between 21 cm and 85 cm (average of 54 \pm 18 cm) over 18 years (2000–2017), with 2003 and 2011 as dry years, and 2006 and 2015 as wet years. The annual loading of calcium and sulfate averaged at 0.19 \pm 0.07 g m⁻² yr⁻¹ and $0.32 \pm 0.11 \text{ g m}^{-2} \text{ yr}^{-1}$, respectively, following the same temporal trend as the annual precipitation (Appendix Fig. 3A). However, the dissolved Ca concentrations in the rain decreased significantly with increasing annual rainfall, indicating the rain was diluted during wet vears ($R^2 = 0.39$; p = 0.01; Appendix Fig. 3B). Two rainwater samples from El Paso, Texas had the same Sr concentrations and isotope ratios ([Sr] = 70 and 72 ppb; 87 Sr/ 86 Sr = 0.70924 and 0.70926 respectively). With Sr concentration at 71 ppb in the rainfall, and annual rainfall of 54 cm, Sr loading was approximately at 38 mg m⁻² yr⁻¹. The Ca/Sr ratio of the rainwater was 0.01 mol/mmol, but this was a rough estimate as Ca and Sr concentrations were measured on rain waters that were collected from El Paso, Texas and Mayhill, New Mexico, ~200 km apart from each other and ~190 km SW and ~60 km S of the study sites, respectively.

White et al. (2015) reported strong linear correlations of Fe and Ca contents and Fe and Sr contents in regional PM_{2.5} dusts (Ca = $1.27 \times \text{Fe}$, and Sr = $0.0117 \times \text{Fe}$) of several IMPROVE sites; however, for the WHIT1 site (Sierra Blanca Regional Airport, NM) adjacent to three of our sampling sites, Ca and Sr in PM2.5 are derived from both regional dust and local dust (i.e., White Sands, Ca* or Sr*). Thus, White Sands Ca* (or Sr*) contents were calculated as the difference between total and that is dust-derived as: $Ca^* = Ca-1.27 \times Fe$. and $Sr^* = Sr-0.0117 \times Fe$ (White et al., 2015). The annual average of PM_{2.5} Ca* and Sr* data (mass/volume air; ng m⁻³) from the IMPROVE WHIT1 site was reported in Appendix Table 1 from 2006 to 2017, and varied also with time (Appendix Fig. 3C). The Ca* and Sr* contents were negatively correlated with annual rainfall (Ca*: R2 = 0.33, p = 0.06; Sr*: $R^2 = 0.43$, p = 0.03; Appendix Fig. 3D), with higher concentrations observed in the drier years. The Sr*/Ca* ratio was similar to those reported in White et al. (2015), with an average mass ratio of 0.07 \pm 0.02 or molar ratio of 0.03 \pm 0.01 mol/mmol.

The mass of the dust collected was 1544 mg (1011 and 533 mg for two periods) at site A, and 1241 mg (603 and 638 mg) at site C. When the mass was normalized to the surface area of the collector (0.14 m²) and the deployment time of the dust collector (370 days at site A and 302 days at site C), the dust deposition rate at our study site was approximately 10.8 g m $^{-2}$ yr $^{-1}$ (10.9 and 10.7 g m $^{-2}$ yr $^{-1}$ at sites A and C, respectively). Given the water-soluble fraction of the dust is known,

the flux of soluble calcium and sulfate through atmospheric input would be 0.10 and 0.14 g m⁻² yr⁻¹, respectively.

5. Discussion

5.1. Separating different end-members for soil chemistry and plant nutrients

In critical zone, soils are ultimately created by alteration of bedrock or parent materials and removed through erosion and leaching (Jin et al., 2010; Aciego et al., 2017), with contribution from atmospheric deposition. For this study, four sites have different bedrock composition and reactivity, but are close enough to receive similar amounts of rainfall and dust inputs, including regional dust from multiple sources (Rivera Rivera et al., 2010; Baddock et al., 2011; Rivas et al., 2018) and a specific local gypsum dust from White Sands (White et al., 2015). Hence, regional dust, gypsum dust, and bedrock are three end-members that control bulk soil chemistry. To be bio-accessible to local vegetation, however, inorganic nutrients have to be present in soluble forms. For example, soluble Ca in the study sites could be contributed from rainfall, soluble fraction of regional dust, gypsum sand, and dissolution of mineral soils. Here, we will use geochemical and isotopic tools to characterize different end-members for bulk soil chemistry and for bioavailable nutrient Ca.

End-member for bedrock inputs is controlled by lithology. Four soil profiles were selected under bedrocks of contrasting weatherability. The most reactive bedrocks were observed at site A (limestone substrate; 93% calcite; ⁸⁷Sr/⁸⁶Sr ratio: 0.7083; Ca/Sr = 2.7 mol/mmol), followed by site C (mixed limestone; ⁸⁷Sr/⁸⁶Sr: 0.7100; Ca/Sr = 0.5 mol/mmol) and by site B (diorite substrate with alkali and plagioclase feldspars; ⁸⁷Sr/⁸⁶Sr: 0.7072; Ca/Sr: 0.1 mol/mmol). The least reactive bedrock was at site D (nearly pure sandstone; ⁸⁷Sr/⁸⁶Sr: 0.7108; Ca/Sr: 0.03 mol/mmol) (Table 2; Fig. 4A).

Bulk dust sample contained mainly quartz, calcite, plagioclase and microcline, with no detectable gypsum (Appendix Fig. 3), and had ⁸⁷Sr/⁸⁶Sr ratio of 0.7087 (Table 2; Fig. 4A) falling within the range of Sr isotopes in the regional dusts of New Mexico (0.7087-0.7092; Capo et al., 1998; Van der Hoven and Quade, 2002; Coble et al., 2015). The dust deposition rate was estimated at 10.8 g m⁻² yr⁻¹, relatively low compared to those reported for other sites in the Chihuahuan Desert: dustfall flux near Las Cruces, New Mexico was estimated at 16 to 59 g m $^{-2}$ yr $^{-1}$ (Gile et al., 1981); Salt Basin, Texas, approximately 50 g m $^{-2}$ yr $^{-1}$ (Perez and Gill, 2009); Hueco Tanks, Texas, 56 g m $^{-2}$ yr⁻¹ (Rivas, 2019), and in urban El Paso, Texas, 111 g m⁻² yr⁻¹ of dust fall (Rivas, 2019). Such a difference in the dustfall is reasonable because a large portion of dust deposition in the Chihuahuan Desert occurs during isolated dust events emanating from lowland basins, making dust deposition heterogeneous spatially and temporally (Perez and Gill, 2009; Rivera Rivera et al., 2010; White et al., 2015). More importantly, the study site dust traps are in a vegetated highland, higher in elevation than the surrounding desert basins and cities where other dust flux measurements were made, and ~100 km distant from the nearest major dust sources (Baddock et al., 2011). All these suggest a lower dust flux is expected, consistent with regional dust fluxes to other highlands in the western USA summarized in Lawrence and Neff (2009). In fact, Gile et al. (1981) measured a dust flux of 12.4 g m $^{-2}$ yr⁻¹ in the Organ Mountains east of Las Cruces, New Mexico at a similar elevation to this study's sites.

White Sands emits sand and dust regularly downwind and becomes an important source of aeolian dust to the Sierra Blanca and Sacramento Mountains (see the dust plume in Fig. 1a; Baddock et al., 2011; White et al., 2015). White et al. (2015) studied elemental fluxes of fine particle dust (PM $_{2.5}$) at the IMPROVE sampling station WHIT1 < 1 km away from our dust trap sites, and reported that gypsum particles contributed approximately 40% of the calcium of the PM $_{2.5}$ dust signal, much higher than what was observed in bulk dust of this study. However, bulk dust collectors deployed in this study collect

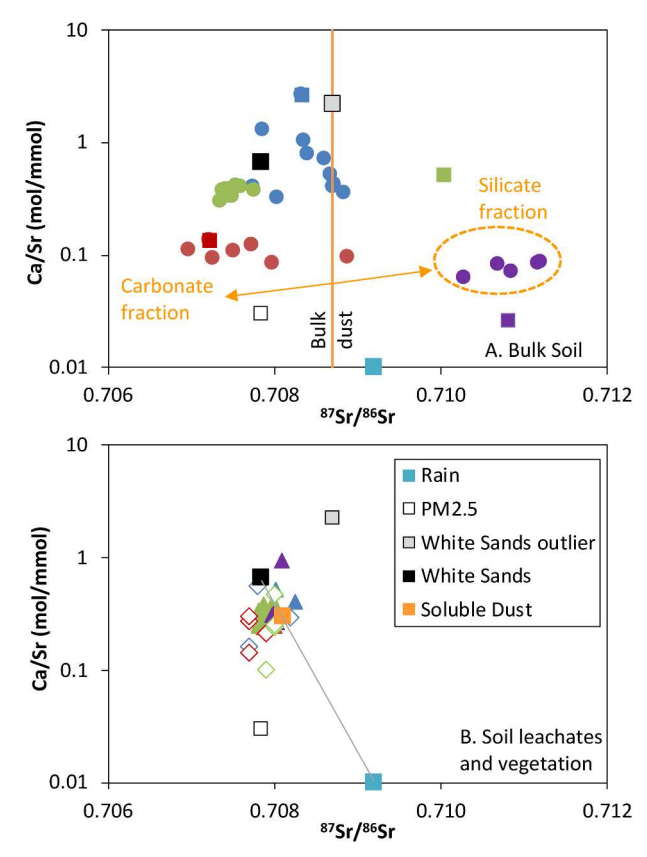


Fig. 4. Correlation of Ca/Sr and 87 Sr/ 86 Sr in (A) bulk soil (solid circles), rock (solid squares), and White Sands samples and (B) all water leachate (open diamonds) and plant samples (triangles). Rain, PM2.5, and dust (soluble) samples are also plotted. Site A = blue, site B = red, site C = green, and site D = purple. (For interpretation of the references to colour in this figure legend, the reader is referred to the web version of this article.)

all falling particles regardless of size. This suggests that silicate and carbonate minerals were in dust as much larger particles than $PM_{2.5}$, while gypsum from White Sands was more important for dust in finer particle fractions. It is consistent with the findings that regional dust storms transported large masses of silt- to sand-sized grains to distant highlands (Lawrence et al., 2010; Neff et al., 2013), and that contemporaneous deposition into the same model of dust traps in El Paso, Texas was dominated by silty and sandy grains with gypsum only rarely detected in individual events (Rivas et al., 2018, 2019).

For eight out of nine White Sands samples, 87Sr/86Sr ratios were uniform around 0.7078-0.7079 (Table 3). Only one of these eight sediments (WSD2) was characterized extensively for Ca/Sr ratios (0.66 mmol/mol), mineralogy (only gypsum detected under XRD) and water soluble chemistry (dominated by dissolved SO_4^{2-} and Ca^{2+}) (Appendix Fig. 1; Table 3), so it is reasonable to assume that bulk sample and water leachable fraction of White Sands have similar ⁸⁷Sr/⁸⁶Sr and Ca/Sr ratios. Interestingly, Ca/Sr ratios of PM_{2.5} particles from White Sands are shown to be close to 0.03 mol/mmol (IMPROVE WHIT1 site; Appendix Table 1; White et al., 2015), much lower than what is observed in the bulk sand in this study. This suggests that substitution of Ca by Sr in gypsum crystals might be dependent on particle sizes or formation mechanisms. Airborne particles from the White Sands as observed in Fig. 1 are a mixture of different sizes and thus have Ca/Sr ratios between 0.03 and 0.66. The Lake Lucero sample is very different from others from the White Sands: ${}^{87}Sr/{}^{86}Sr = 0.7087$; Ca/Sr ratio = 2.19 mmol/mol; the mineral assembly is more complex with gypsum, halite and mirabilite. This is probably due to its unique hydrological characteristics at the Lake Lucero where wetter conditions make it a minor contributor to the dust emission within White Sands.

Rain or snow samples were not collected at the study sites, but rainwater samples from El Paso, Texas, ~190 km from the study sites, had Sr isotopes of 0.70925 (\pm 0.00001) and Ca/Sr ratios of 0.01 mol/mmol (Fig. 4). The precipitation near Las Cruces, New Mexico, 160 km away from the study sites, had $^{87}\text{Sr/}^{86}\text{Sr}$ ratios between 0.7089 and 0.7092, and Ca/Sr ratios variable but lower than 0.36 mol/mmol (Graustein and Armstrong, 1983; Graustein, 1989; Capo and Chadwick, 1999), similar to those of rainwater samples from El Paso, Texas. These ratios were also similar to those of PM_{2.5} particles from IMPROVE site near the White Sands, probably indicating fine White Sands particles dissolved in the rain and modified rain chemistry (Fig. 4B). Indeed, during dry years, Ca* contents (as gypsum) in the PM_{2.5} dust particles are lower and so are Ca concentrations in the rain (Appendix Fig. 3).

The dust traps collected regional and local dust from various sources, gypsum dust from White Sands, and precipitation as snow and rain. Indeed, rainwater or snowmelt was observed at the bottom of dust collector pans. Gypsum was not detected in the bulk dust samples by XRD probably because its content is lower than 5%, the typical detection limit of XRD, and because it dissolved in precipitation falling into the dust traps. This is reasonable given that 2016 and 2017 were normal and wetter years respectively. Gypsum is soluble in water, and thus the water leachable fraction of the dust combines gypsum dust and precipitation end-members. Based on the bulk dust deposition rate and chemistry of the water-soluble fraction, the fluxes of soluble calcium and sulfate were estimated roughly at 0.10 and 0.14 g m $^{-2}$ yr $^{-1}$, on the same order of magnitude as those from wet deposition (0.23 and 0.15 g Ca m $^{-2}$ yr $^{-1}$ and 0.30 and 0.27 g SO₄ m $^{-2}$ yr $^{-1}$, respectively, for year 2016 and year 2017). Dust samples were collected partially for year 2016 and year 2017, and rainfall was not collected at the study sites, so two fluxes could not be directly compared. Even so, it is clear that rainfall and snowmelt contribute to the water-soluble portion of the atmospheric dust deposited in soils, as was documented in the Guadalupe Mountains (~100 km SE of our study sites) by Ponette-González et al. (2018). In the current study, the Ca/Sr ratio in dust leachate was 0.30 mol/mmol with an 87Sr/86Sr ratio of 0.7081 and SO_4^{2-}/Ca^{2+} molar ratio of 0.56, falling within the ranges defined by these two end-members but closer to the White Sands end-member (Fig. 4B). Hence, the dust leachate signature was a mixture consisting primarily of rain and gypsiferous White Sands dust.

5.2. Relative importance of atmospheric inputs and bedrock weathering in controlling soil chemistry

The four study sites are underlain by bedrocks of different reactivities, and thus soil profiles, even assuming similar inputs of dust and rainfall, have different trends of elemental, mineralogical and isotopic composition. At site A, calcite dissolution was the primary control on evolution of bulk soil chemistry and mineralogy as observed through negative τ_{CaO} values, a decrease in inorganic carbon concentrations toward surface, and decrease of intensity of calcite peaks in XRD spectra at shallow soils (Table 2; Appendix Figs. 1 and 2). In contrast, the silicate minerals quartz, plagioclase, and K-feldspar had larger peaks in XRD towards the surface along with an increase in absolute concentrations of their associated elements (K, Al, and Si). The Ca/Sr and 87Sr/86Sr ratios of bulk soils changed with depth and converged on the bedrock values (Fig. 2). Therefore, the Ca/Sr and ⁸⁷Sr/⁸⁶Sr ratios observed at surface were indicative of silicate mineral end-member and at depth - Ca/Sr and 87Sr/86Sr ratio modification indicated a mixing of carbonate and silicate mineral end-members (Fig. 4). The dust signature was not detectable in bulk soils. Soils at site C contained calcite and silicate minerals and behaved differently from those at site A. Here, carbonate-bearing elements (Ca, Mg, and Sr) all showed immobile depth profiles within uncertainties (Table 2; Appendix Fig. 2), suggesting that calcite dissolution has predominantly occurred to disintegrate the bedrock at the bedrock-soil interface as observed by dramatic shifts in Ca/Sr ratio and 87Sr/86Sr (Fig. 2). Carbonate

weathering at site C was not so extensive as that at site A, probably because of its lower calcite to silicate mineral ratio, and thus less exposure of calcite to infiltrating water. In summary, calcite weathers quickly at site A, depleting Ca towards soil surface and making its addition from dust invisible through bulk soil analysis.

The soil profiles at site B were developed on diorite with relatively low CaO concentrations (Table 2). The primary Ca-bearing mineral in the diorite was plagioclase (Appendix Fig. 1B), but weathering of plagioclase was slow as observed by immobile Ca profiles and little variation in the Ca/Sr ratios (Fig. 2A; Appendix Fig. 2B). Both Ca/Sr and $^{87}\text{Sr}/^{86}\text{Sr}$ ratios at shallower soils shifted towards dust and White Sands end-members, indicative of dust inputs (Fig. 4). The soils at site D were developed on sandstone with low CaO contents and minimal chemical weathering; variation in soil chemistry was controlled by dust inputs. Indeed, slightly positive τ values indicated that CaO, Sr, MgO and Na₂O were enriched in soils (Appendix Fig. 2D); the Ca/Sr remained relatively constant but the $^{87}\text{Sr}/^{86}\text{Sr}$ ratios decreased gradually towards the atmospheric end members at soil surface, indicating that atmospheric deposition dominated chemistry at this site (Fig. 2).

No elemental concentration data (thus Ca/Sr ratio) were collected for bulk dust due to the small sample size, except for Sr isotopes (Fig. 4A). However, the soil chemistry can shed some light on the dust characteristics. Indeed, shallow soils at site D have positive Ca and Sr mass transfer coefficients (τ values), indicating dominant dust inputs of these two elements over bedrock (Appendix Fig. 2D). Carbonate, present in the dust as observed through XRD (Appendix Fig. 1), was not detected in the soil profiles at site D, suggesting calcite quickly dissolved. If so, shallow soils at site D represent the silicate fraction of the dust with Ca/Sr ratios between 0.06 and 0.09 mol/mmol and 87 Sr/ 86 Sr around 0.711, whereas the soluble carbonate or sulfate fraction of dust would have slightly a lower 87 Sr/ 86 Sr ratio than that of the bulk dust (0.7087).

5.3. Calcium uptake by vegetation: Different sources of mineral nutrients

The leaching of a soil by water allows isolation of the gypsum dusts and investigation of its mobility in the critical zone. The soil leachates in all sites were dominated by ${\rm Ca}^{2+}$ and ${\rm SO_4}^{2-}$, consistent with the chemistry of White Sands gypsum (Table 3; Fig. 3). Concentrations of these soluble ions generally increased down profile in all sites, largely attributed to a sharp decrease in permeability at soil-bedrock interface. For sites C and D with lower degrees of mineral weathering and soil development, high ${\rm Ca}^{2+}$ concentrations in soil leachates were observed at soil surface.

The same narrow range of Ca/Sr ratios was observed in soil leachates for all four sites, independent of the bedrock lithology, suggesting common atmospheric source(s) for Ca and Sr (Fig. 2D). Indeed, the Ca/Sr ratios of these leachates fell out of those of the mineral soils at each site, but were close to that of soluble dust, and within the two atmospheric end-members: rain and White Sands dust (Fig. 4B). This is reasonable given that soluble Ca²⁺ from soil mineral dissolution is limited due to slow dissolution kinetics of silicate and carbonate phases in comparison to evaporite salts like gypsum (Miller et al., 2014; Brantley et al., 2007). Similarly, the ⁸⁷Sr/⁸⁶Sr of soil leachates was uniform among all four sites, and fell within those of two atmospheric end-members (Fig. 2C; White Sands gypsum: 0.7078, rain: 0.7092, and water soluble fraction of the dust: 0.7081). Thus, the majority, if not all, of the water-soluble Ca and Sr in soils can be explained by the two atmospheric end members.

The Ca/Sr ratios of soil leachates were higher at surface and decreased sharply with depth (Fig. 2D). This strong depth trend could be due to different reasons: first, each dust storm or rainfall event is typically episodic, loading Ca and Sr at soil surface with unique Ca/Sr ratios; the deep soils however integrate all atmospheric inputs over the long term and thus have a uniform Ca/Sr signature. Second, as discussed below, the Ca/Sr ratios of soil leachates can be modified by biological uptakes. The similar Sr isotope ratios of all soil leachates seem to strongly support the latter as vegetation may fractionate Ca and

Sr but not Sr isotopes at detectable levels.

Ca/Sr and 87Sr/86Sr ratios have been used to identify calcium sources in vegetation (Capo and Chadwick 1999; Huntington et al., 2000; Dasch et al., 2006; Nezat et al. 2008; Pett-Ridge et al., 2009a,b; Jin et al., 2012; Miller et al., 2014; Burger and Lichtscheidl, 2019). In this study, the ⁸⁷Sr/⁸⁶Sr ratios of the plant samples had a narrow range between 0.7077 and 0.7082 with an outlier 0.7090 at Site D (grass). The overall ranges are very similar to those of the soil leachates (Table 4; Fig. 2C). This narrow range independent of sites is logical considering that water soluble or exchangeable nutrients are often considered as biologically available (Gosz and Moore, 1989; Coble et al., 2015). Plants in the Sangre de Cristo Mountain range to the north had higher ⁸⁷Sr/⁸⁶Sr ratios than those observed in this study, because regional background dust from the Colorado Plateau are distinctively different from signatures observed at the study sites (Table 4; Gosz and Moore, 1989; Capo and Chadwick, 1999; White et al., 2015). This indicates that transport and deposition of White Sands particles as dust are driven by prevailing wind direction and distance, and different sources of dust may impact the isotopic chemistry of plants at receptor sites downwind. Similarly, Ca/Sr ratios in plants were also clustered regardless of bedrock. All Ca/Sr ratios measured on plant samples were below 0.55 mol/mmol, with the majority below 0.35 mol/mmol (Table 3; Fig. 2D). These were well between Ca/Sr ratios of the two end members - White Sands and precipitation - and close to Ca/Sr ratios of the soil leachates. Therefore, most of Ca and Sr taken up by plants were atmospherically derived, similar to the signatures of the water leachable fraction of the soils as previously discussed. Variation in Ca/Sr ratios were better explained by vegetation types and not by sites. For example, the Ca/Sr ratios of all plants at site A were scattered at 0.33 ± 0.20 mol/mmol but the Ca/Sr ratios of all grasses among four sites were 0.25 ± 0.04 mol/mmol (Table 4). The Ca/Sr ratios of conifer samples were generally the lowest of all plant species (0.11-0.16, n = 4, with an outlier of 0.30 mol/mmol at Site B; Table 4).

The rooting depth of conifers was deepest of all the plant types in this study; in fact, Juniperus monosperma, the dominant tree at the study sites, has been identified as one of the most deeply-rooted trees in North America (Stone and Kalisz, 1991; Adler et al., 2009). Thus, it was reasonable to conclude that nutrients such as Ca were taken up by conifers from deeper soils, at the soil-bedrock interface, where Ca/Sr ratios of the soil leachates and influence of dust influx in the soil water were the lowest of all. In addition, ⁸⁷Sr/⁸⁶Sr ratios of conifers were also among the lowest of all species, similar to those of the deepest soil leachates. The Ca/Sr ratios in shrubs were higher than those in conifers and varied more among sites, ranging from 0.25-0.55 mol/mmol (Table 3). Shrubs had shallower roots than conifers, and thus received nutrients at mid-soil layers, where Ca/Sr ratios of soil leachates were higher than those at depths. Different from conifers, shrubs had large variations in both Ca/Sr and ⁸⁷Sr/⁸⁶Sr ratios (0.7077-0.7081), probably due to the different species of shrubs with different physiologies and rooting habits that were visually observed at each site and thus sampled. The rooting depth of the grass was the shallowest of all plants, and the Ca/Sr ratios varied from 0.21 to 0.29 mol/mmol in grass samples, much higher than those observed in leachates of shallow soils. Grass samples had the most variable 87Sr/86Sr ratio between 0.7079 and 0.7090, always equal to or higher than the 87Sr/86Sr ratios of other plants at the same site (Table 4). The variation in elemental ratios and isotopic ratios suggested that the Ca and Sr in grasses may be dependent on short-term rain or dust deposition, as being more susceptible to seasonal variation in water and nutrient source and chemistry. The grass samples therefore demonstrated smaller-scale spatiotemporal variability from atmospheric inputs, as they harvested calcium from recent deposition events.

The discussion above assumes that rooting depth controls the exact depth of soils where nutrients are taken and thus what Ca/Sr signatures are acquired. Alternatively, roots could preferentially uptake certain elements. A previous study at Hubbard Brook Experimental Forest had

identified preferential uptake of Ca over Sr in the foliage and this enrichment factor was different among different tree species (Dasch et al., 2006). Interestingly, concentrations of other elements Fe, Na, Mn, and Mg in leaves of these plants varied more between sites than between plant types in this study (Table 4). If so, soil Ca and Sr can be fractionated during biological uptake in gymnosperms, shrubs, and cacti, and again during the leaf falls. This could explain why Ca/Sr ratios of grass samples did not follow the depth trends of shrubs and gymnosperms, possibly as grasses fractionate these two elements during uptake. However, the ⁸⁷Sr/⁸⁶Sr ratios are not fractionated at the same level due to slow decay of ⁸⁷Rb to ⁸⁷Sr, and thus their isotope ratios in the soil leachates and vegetation types are more uniform with depth than Ca/Sr ratios.

6. Conclusions

We investigated the impacts of a unique dust source, the gypsum particles from White Sands National Monument on soil profiles downwind in the far northern Sacramento Mountains, New Mexico. Four soil profiles were sampled on four different bedrock types with contrasting reactivity, and analyzed for elemental chemistry, mineralogy, and water leaching fraction. In addition, representative samples from White Sands, bulk dust, rainfall data from NADP sites, and local bedrocks were collected to constrain the inputs of soluble nutrients to the critical zone. We focused on deposition and mobility of the gypsum dust in the active critical zone, and evaluated its contribution to Ca as nutrients in plants using Sr/Ca and ⁸⁷Sr/⁸⁶Sr ratios.

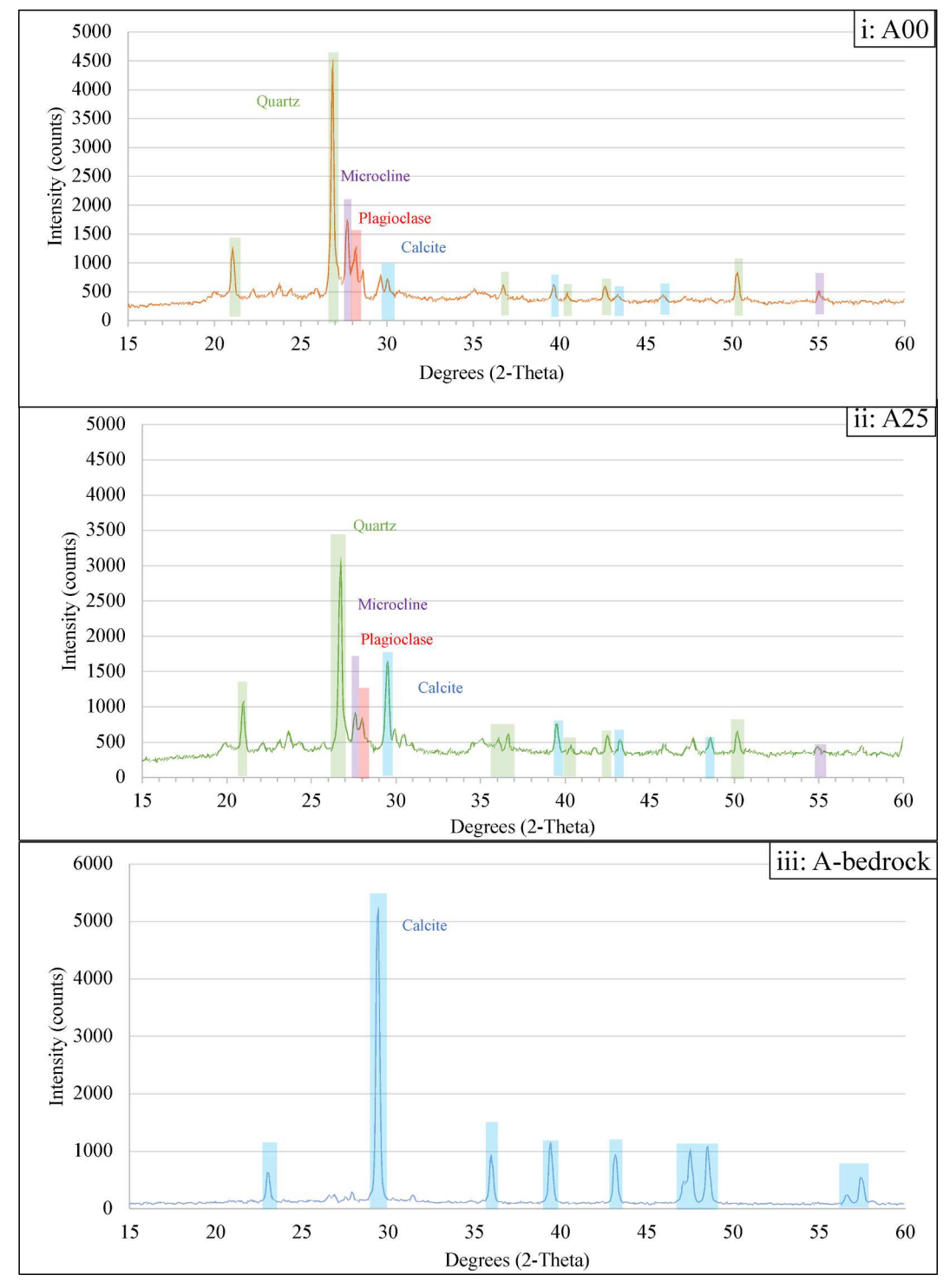
Bulk soil chemistry and mineralogy including Sr isotopes were predominantly governed by long-term chemical weathering, especially dissolution of soluble calcite in the bedrock. Only in the least weathered sandstone, where initial CaO wt% is very low, could atmospheric inputs be detected in shallow soils. In contrast, the elemental chemistry, Sr/Ca and ⁸⁷Sr/⁸⁶Sr ratios of soil leachates were similar among all four soil profiles, indicative of a common atmospheric deposition, with combined rainfall and gypsum dust inputs. The leaves of plants, including those of conifers, cacti, grass and shrubs, also had similar Sr/Ca and 87Sr/86Sr ratios as soil leachates among four sites, suggesting the same atmospheric inputs. Interestingly, the Sr/Ca ratios of different plants vary more uniformly as plant types, instead of sites, probably controlled by their rooting depth or/and by taxon specific Sr/Ca partitioning during nutrient uptake. Gypsum was not detectable in bulk soils or insoluble fraction of the dust, suggesting that it was highly mobile and transported quickly through soils via fast dissolution. Indeed, most soil leachates showed increasing concentrations of dissolved Ca²⁺ and SO₄²⁻ with depth until bedrock-soil interface, where permeability decreased sharply.

Acknowledgements

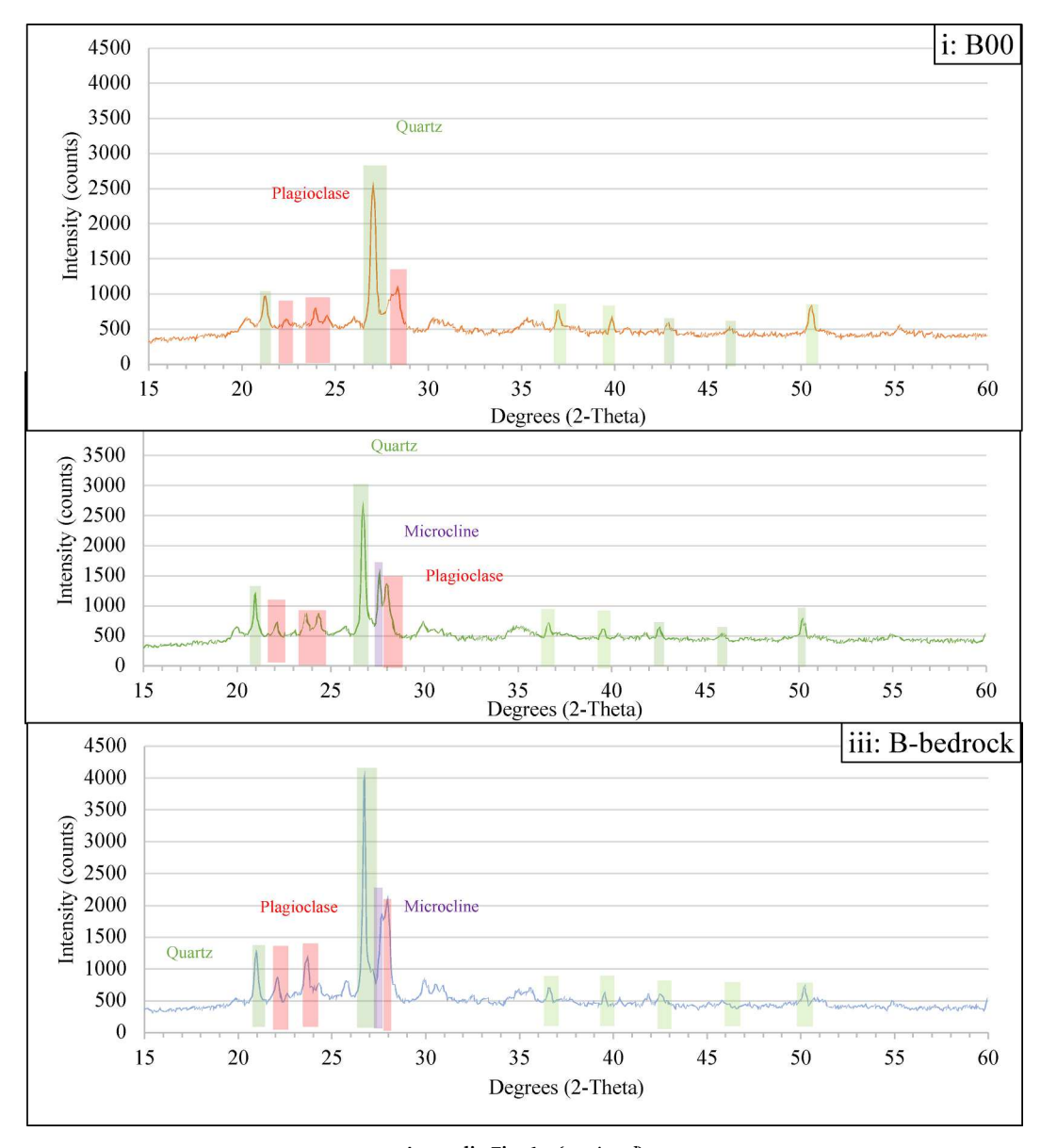
We are thankful for all the assistance in the laboratory at the Department of Geological Sciences, University of Texas at El Paso from Sandra Garcia, Anna Ortiz, Syprose Nyachoti, Mercedes Navarro-O'Hara, Joe Rivas, Jaime Enriquez, Karen Valles, and Victor Garcia. We also would like to acknowledge all the assistance in the field from Alex Eddy, Nick Tischio, and Joann Pinkley. Special thanks go to David Bustos and other staff at the White Sands National Monument for their help in facilitating sample collection at White Sands. We thank Dr. Zhuping Sheng from the Texas AgriLife Research Center at El Paso for providing the archived rainwater samples. All data for this paper are presented in Tables or Appendix Tables. IMPROVE is a collaborative association of state, tribal, and federal agencies, and international partners. The U.S. Environmental Protection Agency is the primary funding source, with contracting and research support from the National Park Service. The Air Quality Group at the University of California, Davis, is the central analytical laboratory, with ion analysis provided by the Research Triangle Institute and carbon analysis provided by the Desert Research Institute. TEG acknowledges support from NASA grant NNX16AH13G.

Appendix 1

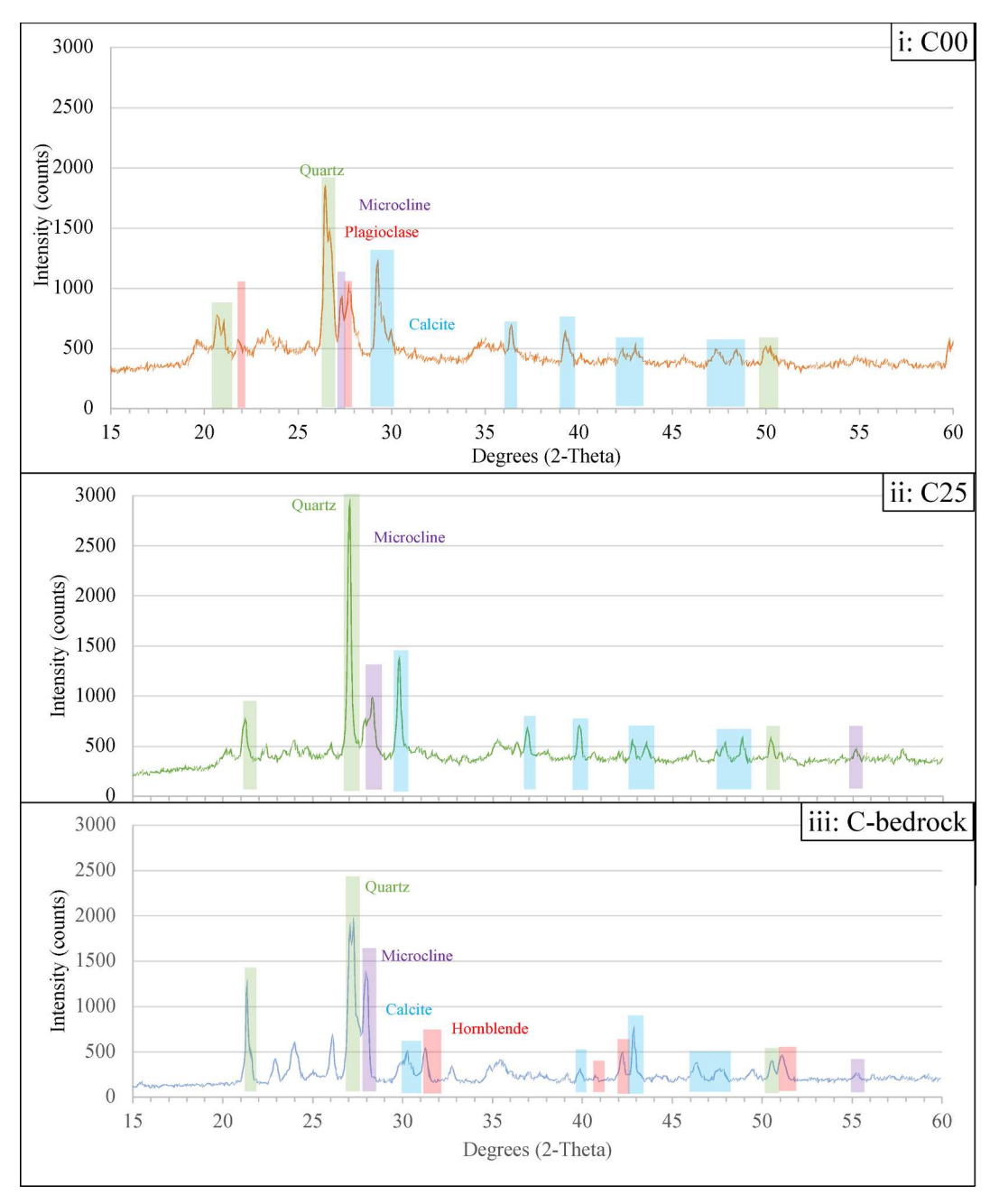
See Appendix Figs. 1-3 and Table 1.



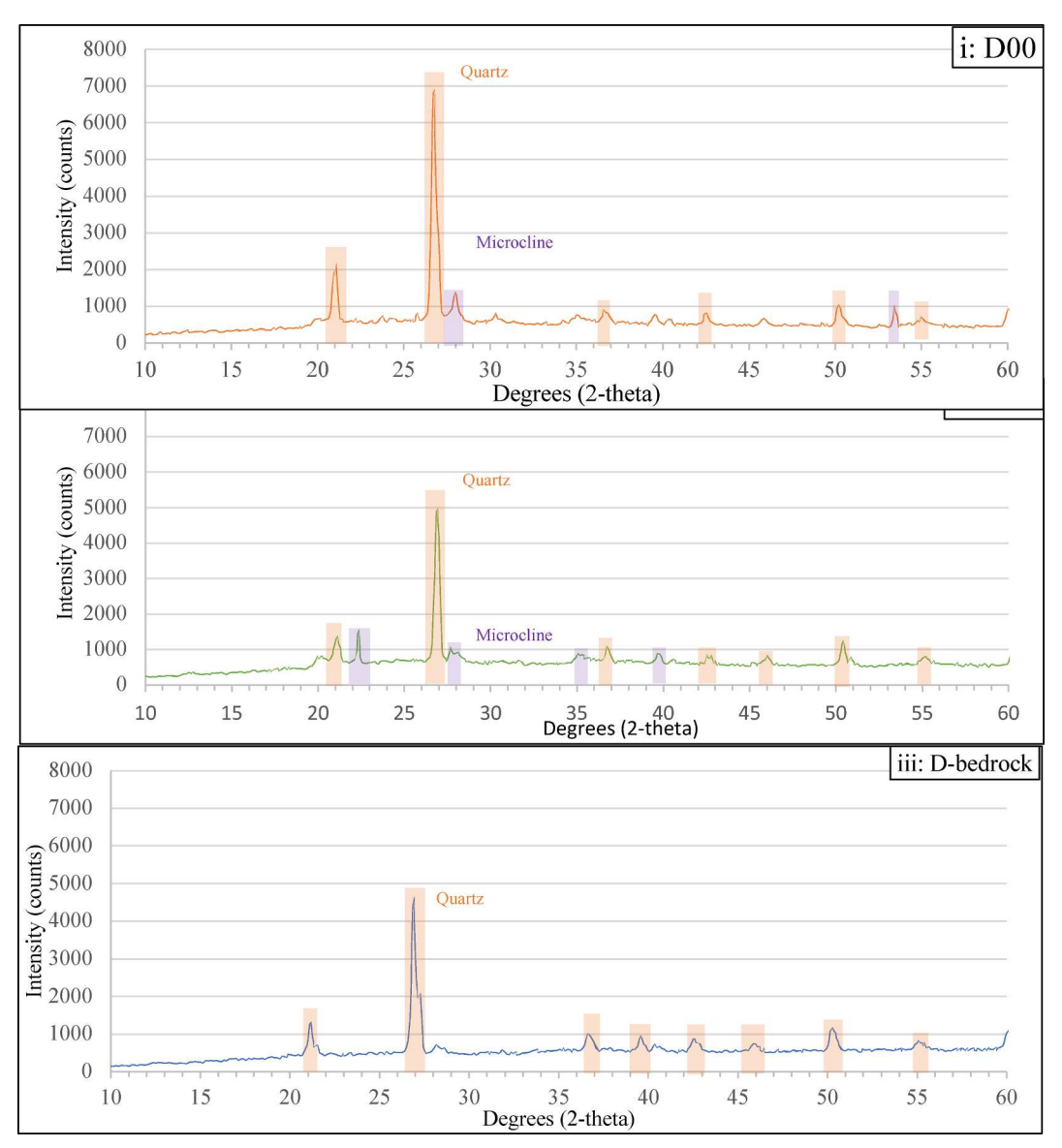
Appendix Fig. 1. Major minerals identified in soils and bedrock at Site A (i: A00, ii: A25, and iii: A-bedrock), Site B (i:B00, ii: B15, and iii: B-bedrock), Site C (i: C00, ii: C25, and iii: Cbedrock), Site D (i: D00, ii: D10, and iii: D-bedrock), and major minerals identified in White Sands samples (i: WSD1, Lake Lucero sediments, and ii: WSD2, parabolic dune crest), and bulk dust.



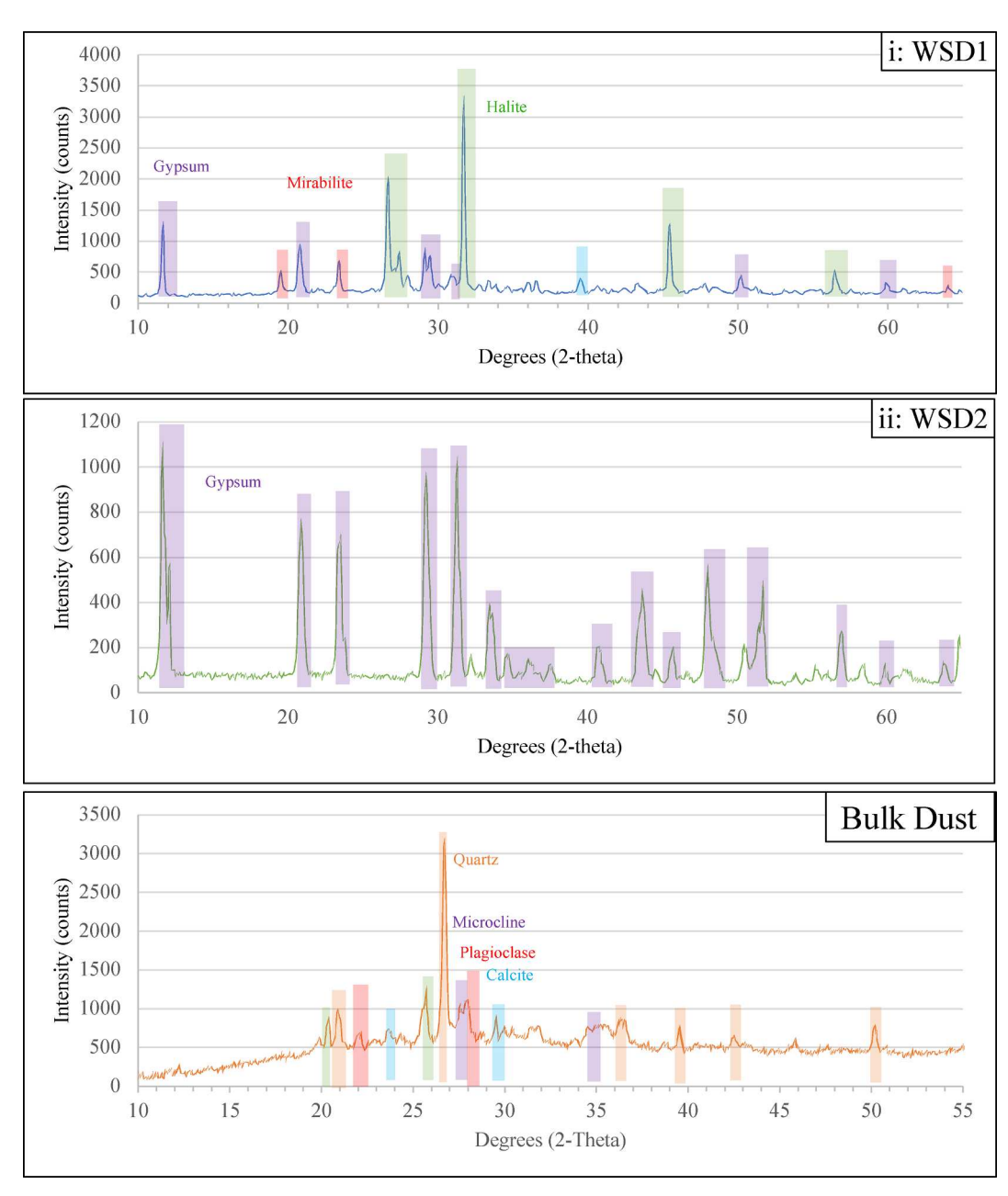
Appendix Fig. 1. (continued)



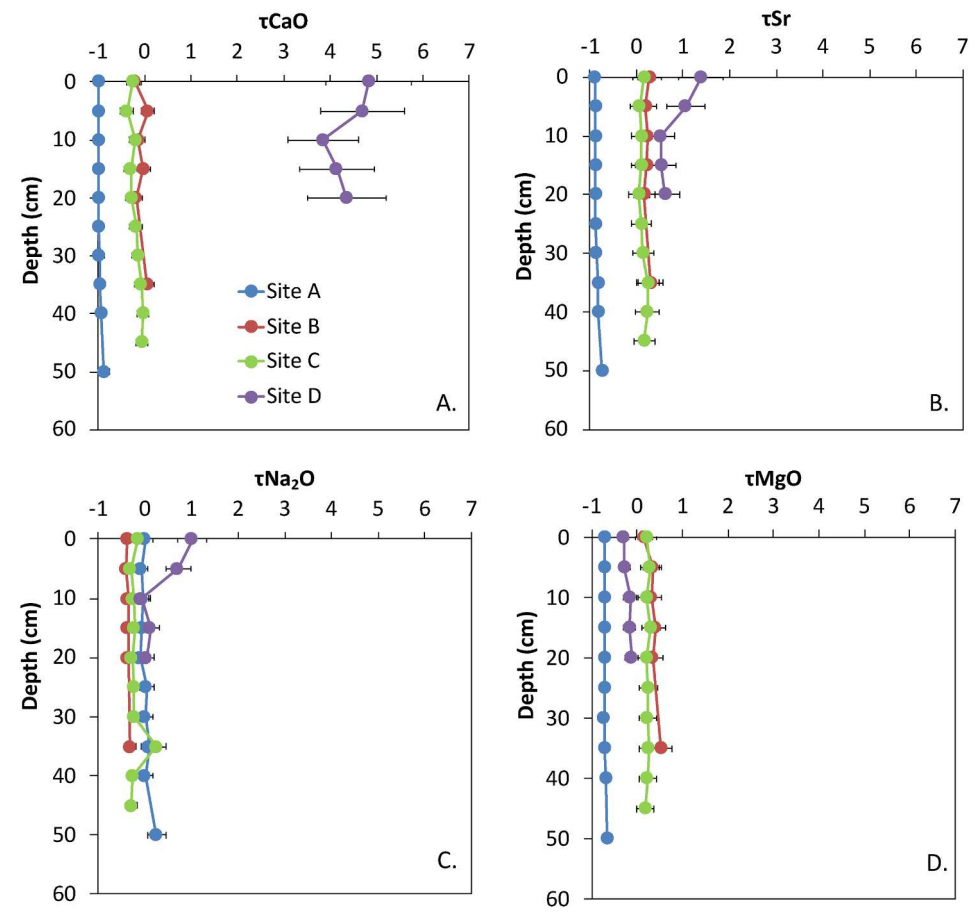
Appendix Fig. 1. (continued)



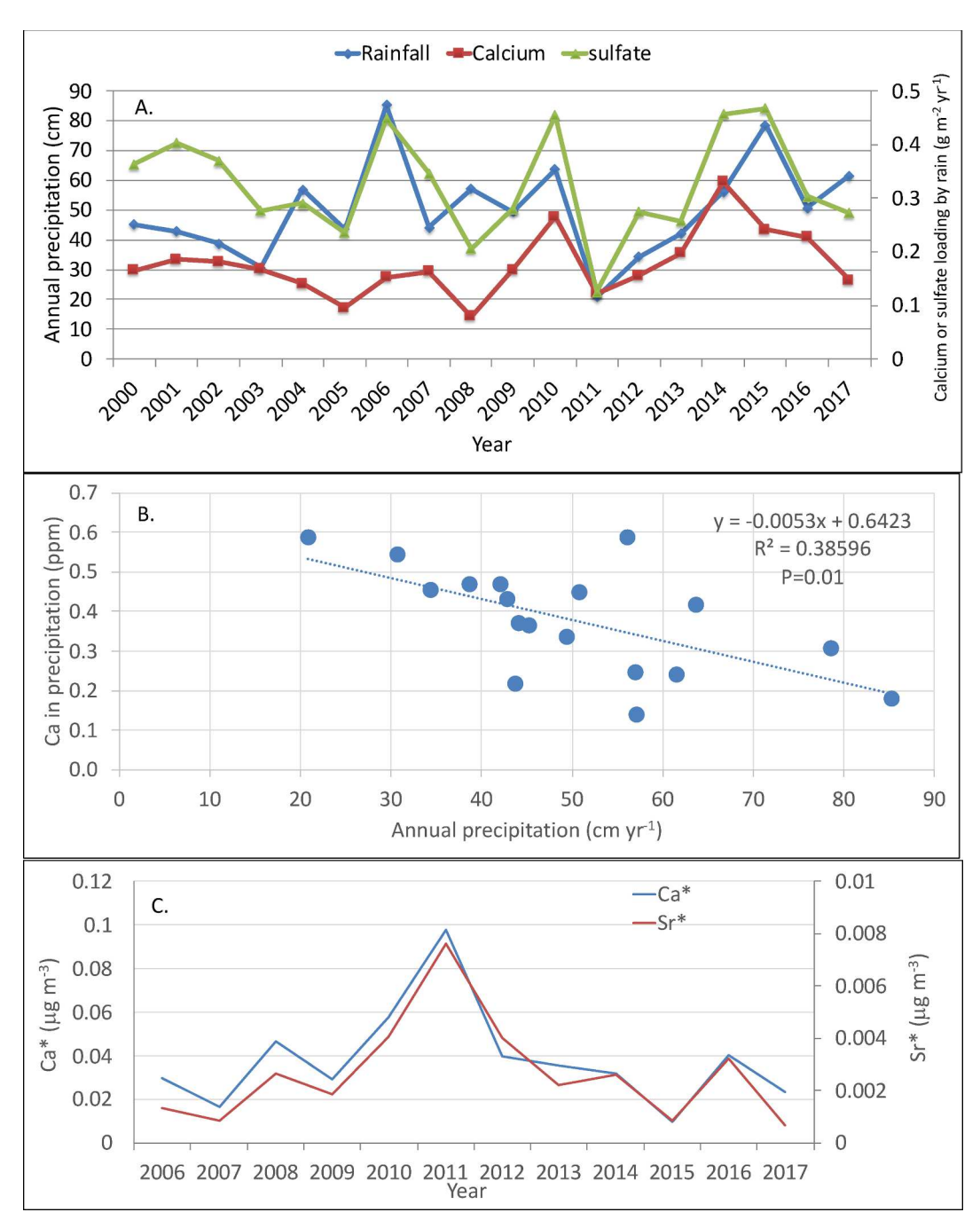
Appendix Fig. 1. (continued)



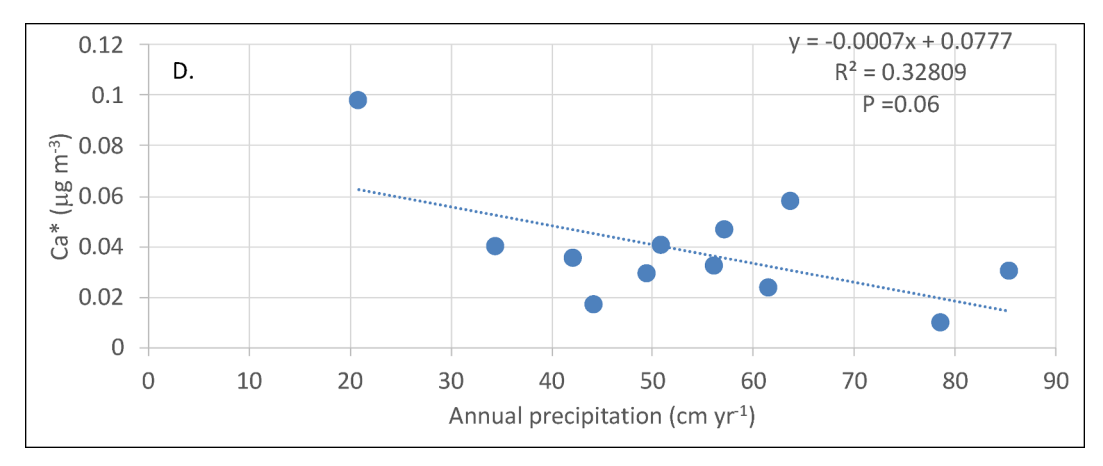
Appendix Fig. 1. (continued)



Appendix Fig. 2. Depth variation in mass balance transfer coefficient τ of (A) CaO, (B) Sr, (C) Na₂O, and (D) MgO at four soil profiles.



Appendix Fig. 3. (A) Variation of rainfall, Ca loading, and sulfate loading over time; (B) Ca concentrations in rainfall decreases significantly with rain amount; (C) Gypsum derived Ca* and Sr* concentrations in PM2.5 over time, and (D) they typically decrease with rainfall amount too. Data accessed from IMPROVE WHIT1 site (http://vista.cira.colostate.edu/improve/).



Appendix Fig. 3. (continued)

Appendix Table 1 Annual loading of calcium and sulfate through $PM_{2.5}$ dust and precipitation.

Year	IMPROVE d	lust flux		NADP precipitation	NADP precipitation							
	Ca* μg/m³	Sr* μg/m³	Ca*/Sr* mole/mmole	Annual precipitation cm	Ca ²⁺ loading g m ⁻² yr ⁻¹	SO ₄ ²⁻ loading g m ⁻² yr ⁻¹	Ca ²⁺ concentrations ppm					
2000				45.2	0.17	0.36	0.36					
2001				42.9	0.19	0.40	0.43					
2002				38.7	0.18	0.37	0.47					
2003				30.7	0.17	0.28	0.54					
2004				57.0	0.14	0.29	0.25					
2005				43.7	0.10	0.24	0.22					
2006	0.030	0.0013	0.049	85.3	0.15	0.45	0.18					
2007	0.017	0.0009	0.042	44.2	0.16	0.35	0.37					
2008	0.046	0.0026	0.038	57.2	0.08	0.21	0.14					
2009	0.029	0.0019	0.034	49.4	0.17	0.28	0.34					
2010	0.058	0.0041	0.031	63.7	0.27	0.46	0.42					
2011	0.098	0.0076	0.028	20.9	0.12	0.13	0.59					
2012	0.040	0.0040	0.022	34.4	0.16	0.28	0.45					
2013	0.035	0.0022	0.035	42.1	0.20	0.26	0.47					
2014	0.032	0.0026	0.026	56.1	0.33	0.46	0.59					
2015	0.010	0.0008	0.025	78.5	0.24	0.47	0.31					
2016	0.040	0.0032	0.027	50.9	0.23	0.30	0.45					
2017	0.023	0.0007	0.076	61.5	0.15	0.27	0.24					

Ca* and Sr*, from gypsum, are calcuted from total Ca, Fe, Sr according to White et al. (2015).

References

Aarons, S.M., Arvin, L.J., Aciego, S.M., Riebe, C.S., Johnson, K.R., Blakowski, M.A., Koornneef, J.M., Hart, S.C., Barnes, M.E., Dove, N., Botthoff, J.K., 2019. Competing droughts affect dust delivery to Sierra Nevada. Aeolian Research 41, 100545.

Abouchami, W., Näthe, K., Kumar, A., Galer, S.J.G., Jochum, K.P., Williams, E., Horbe, A.M.C., Rosa, J.W.C., Balsam, W., Adams, D., Mezger, K., Andreae, M.O., 2013. Geochemical and isotopic characterization of the Bodélé Depression dust source and implications for transatlantic dust transport to the Amazon Basin. Earth and Planetary Science Letters 380, 112–123.

Aciego, S.M., Riebe, C.S., Hart, S.C., Blakowski, M.A., Carey, C.J., Aarons, S.M., Dove, N.C., Botthoff, J.K., Sims, K.W.W., Aronson, E.L., 2017. Dust outpaces bedrock in nutrient supply to montane forest ecosystems. Nature Communications 8, 14800.

Adler, P., Cumming, J., Arora, R., 2009. Nature of mineral nutrient uptake by plants. In: In: Lal, R. (Ed.), Agricultural Science, vol. 1. Eolss Publishers, Oxford, pp. 355–371.

Allmendinger, R., Titus, F., 1973. Regional Hydrology and Evaporative Discharge as a Present-Day Source of Gypsum at White Sands National Monument, New Mexico, New Mexico Bureau of Mines and Mineral Resources, Open File Report 55.

Anderson, S.P., Dietrich, W.E., Brimhall, G.H., 2002. Weathering profiles, mass-balance analysis, and rates of solute loss: linkage between weathering and erosion in a small, steep catchment. Geological Society of American Bulletin 114, 1143–1158.

Arendt, C.A., Aciego, S.M., Hetland, E.A., 2015. An open source Bayesian Monte Carlo isotope mixing model with applications in Earth surface processes: BMC Isotope Mixing model: Earth surface. Geochemistry, Geophysics, Geosystems 16 (5), 1274–1292.

Arvin, L.J., Riebe, C.S., Aciego, S.M., Blakowski, M.A., 2017. Global patterns of dust and bedrock nutrient supply to montane ecosystems. Science Advances 3 (12), eaao1588. Baddock, M.C., Gill, T.E., Bullard, J.E., Dominguez Acosta, M., Rivera Rivera, N.I., 2011. Geomorphology of the Chihuahuan Desert based on potential dust emissions. Journal of Maps 7 (1), 249–259.

Baddock, M.C., Ginoux, P., Bullard, J.E., Gill, T.E., 2016. Do MODIS-defined dust sources have a geomorphological signature? Geophysical Research Letters 43 (6), 2606–2613.

Barkley, A.E., Prospero, J.M., Mahowald, N., Hamilton, D.S., Popendorf, K.J., Oehlert, A.M., Pourmand, A., Gatineau, A., Panechou-Pulcherie, K., Blackwelder, P., Gaston, C.J., 2019. African biomass burning is a substantial source of phosphorus deposition to the Amazon, tropical Atlantic Ocean, and Southern Ocean. Proceedings of the National Academy of Sciences 116 (33), 16216–16221.

Boy, J., Wilcke, W., 2008. Tropical Andean forest derives calcium and magnesium from Saharan dust. Global Biogeochemical Cycles 22 (1). https://doi.org/10.1029/ 2007GB002960.

Bozlaker, A., Prospero, J.M., Fraser, M.P., Chellam, S., 2013. Quantifying the contribution of long-range Saharan dust transport on particulate matter concentrations in Houston, Texas, using detailed elemental analysis. Environmental Science and Technology 47 (18), 10179–10187.

Brantley, S.L., Goldhaber, M.B., Ragnarsdottir, K.V., 2007. Crossing disciplines and scales to understand the critical zone. Elements 3 (5), 307–314.

Brimhall, G.H., Dietrich, W.E., 1987. Constitutive mass balance relations between chemical composition, volume, density, porosity, and strain in metosomatic hydrochemical systems: results on weathering and pedogenesis. Geochimica et Cosmochimica Acta 51, 567–587.

Bristow, C.S., Hudson-Edwards, K.A., Chappell, A., 2010. Fertilizing the Amazon and equatorial Atlantic with West African dust: African fertilizer for Amazon and Atlantic. Geophysical Research Letters 37 (14). L14807.

Burger, A., Lichtscheidl, I., 2019. Strontium in the environment: review about reactions of

- plants towards stable and radioactive strontium isotopes. Science of the Total Environment 653, 1458–1512.
- Capo, R.C., Chadwick, O.A., 1999. Sources of strontium and calcium in desert soil and calcrete. Earth and Planetary Science Letters 170 (1), 61–72.
- Capo, R.C., Stewart, B.W., Chadwick, O.A., 1998. Strontium isotopes as tracers of ecosystem processes: theory and methods. Geoderma 82 (1–3), 197–225.
- Chadwick, O.A., Derry, L.A., Vitousek, P.M., Huebert, B.J., Hedin, L.O., 1999. Changing sources of nutrients during four million years of ecosystem development. Nature 397, 491–497 (Climate data for cities worldwide – Climate-Data.org).
- Coble, A.A., Hart, S.C., Ketterer, M.E., Newman, G.S., Kowler, A.L., 2015. Strontium source and depth of uptake shifts with substrate age in semiarid ecosystems. Journal of Geophysical Research: Biogeosciences 120, 1069–1077.
- Dasch, A.A., Blum, J.D., Eagar, C., Fahey, T.J., Driscoll, C.T., Siccama, T.G., 2006. The relative uptake of Ca and Sr into tree foliage using a whole-watershed calcium addition. Biogeochemistry 80, 21–41. https://doi.org/10.1007/s10533-005-6008-z.
- De Angelis, M., Guidichet, A., 1991. Saharan dust deposition over Mont Blanc (French Alps) during the last 30 yr. Tellus 43B, 61–75.
- Derry, L.A., Chadwick, O.A., 2007. Contributions from Earth's atmosphere to soils. Elements 3, 333–338.
- Ewing, S.A., Sutter, B., Owen, J., Nishiizumi, K., Sharp, W., Cliff, S.S., Perry, K., Dietrich, W., McKay, C.P., Amundson, R., 2006. A threshold in soil formation at Earth's arid-hyperarid transition. Geochimica et Cosmochimica Acta 70, 5293–5322.
- Farmer, A.M., 1993. The effects of dust on vegetation—a review. Environmental Pollution 79 (1), 63–75.
- Feldman, C., 1983. Behavior of trace refractory minerals in the lithium metaborate fusionacid dissolution procedure. Analytical Chemistry 55 (14), 2451–2453.
- Field, J.P., Belnap, J., Breshears, D.D., Neff, J.C., Okin, G.S., Whicker, J.J., Painter, T.H., Ravi, S., Reheis, M.C., Reynolds, R.L., 2010. The ecology of dust. Frontiers in Ecology and the Environment 8 (8), 423–430.
- Fryberger, S., 2001. Geological Overview of White Sands National Monument, accessible at http://nature.nps.gov/geology/parks/whsa/geows/index.htm.
- Galy, A., France-Lanord, C., Derry, L.A., 1999. The strontium isotopic budget of Himalayan rivers in Nepal and Bangladesh. Geochimica et Cosmochimica Acta 63, 1905–1925.
- Gile, L.H., Hawley, J.W., Grossman, R.B., 1981, Soils and geomorphology in the Basin and Range area of Southern New Mexico-Guidebook to the Desert Project, New Mexico Bureau of Mines & Mineral Resources Memoir 39.
- Gill, T.E., 1996. Eolian sediments generated by anthropogenic disturbance of playas: human impacts on the geomorphic system and geomorphic impacts on the human system. Geomorphology 17 (1–3), 207–228.
- Gosz, J.R., Moore, D.I., 1989. Strontium isotope studies of atmospheric inputs to forested watersheds in New Mexico. Biogeochemistry 8 (2), 115–134.
- Graustein, W.C., 1989. ⁸⁷Sr/⁸⁶Sr ratios measure the source and flow of strontium in terrestrial ecosystems. In: Rundel, P.W., Ehleringer, J.R., Nagy, K.A. (Eds.), Stable Isotopes in Ecological Research (vol. 68). Springer-Verlag, New York, pp. 491–512.
- Graustein, W.C., Armstrong, R.L., 1983. The use of strontium-87/strontium-86 ratios to measure atmospheric transport into forested watersheds. Science 219 (4582), 289–292
- Hahnenberger, M., Nicoll, K., 2012. Meteorological characteristics of dust storm events in the eastern Great Basin of Utah, U.S.A. Atmospheric Environment 60, 601–612.
- Hand, J.L., Copeland, S.A., Day, D.E., Dillner, A.M., Indresand, H., Malm, W.C., McDade, C.E., Moore, C.T., Pitchford, M.L., Schichtel, B.A., Watson, J.G., 2011. Spatial and Seasonal Patterns and Temporal Variability of Haze and its Constituents in the United States: Report V. http://vista.cira.colostate.edu/improve/Publications/Reports/2011/2011.htm.
- Hanks, J.P., Dick-Peddie, W.A., 1974. Vegetation patterns of the White Mountains, New Mexico. The Southwestern Naturalist 18 (4), 371–381.
- Hoidale, G.B., Smith, S.M., 1968. Analysis of the giant particle component of the atmosphere over an interior desert basin. Tellus 20 (2), 251–268.
- Huneeus, N., Schulz, M., Balkanski, Y., Griesfeller, J., Prospero, J., Kinne, S., Bauer, S., Boucher, O., Chin, M., Dentener, F., Diehl, T., Easter, R., Fillmore, D., Ghan, S., 2011. Global dust model intercomparison in AeroCom phase I. Atmospheric Chemistry and Physics 11 (15), 7781–7816.
- Huntington, T.G., Hooper, R.P., Johnson, C.E., Aulenback, B.T., Cappellato, R., Blum, A.E., 2000. Calcium depletion in a southeastern United States forest ecosystem. Soil Science Society of America Journal 64, 1845–1858.
- Jacobson, A.D., Blum, J.D., 2000. Ca/Sr and ⁸⁷Sr/⁸⁶Sr geochemistry of disseminated calcite in Himalayan silicate rocks from Nanga Parbat: influence on river-water chemistry. Geology 28, 463–466.
- Jiao, L., Wang, X., Li, D., 2018. Spatial variation in the flux of atmospheric deposition and its ecological effects in arid Asia. Aeolian Research 32, 71–91.
- Jin, L., Ravella, R., Ketchum, B., Bierman, P.R., Heaney, P., White, T., Brantley, S.L., 2010. Mineral weathering and elemental transport during hillslope evolution at the Susquehanna/Shale Hills Critical Zone Observatory. Geochimica et Cosmochimica Acta 74, 3669–3691.
- Jin, L., Mukasa, S.B., Hamilton, S.K., Walter, L.M., 2012. Impacts of glacial/interglacial cycles on continental rock weathering inferred using Sr/Ca and ⁸⁷Sr/⁸⁶Sr ratios in Michigan watersheds. Chemical Geology 300–301, 97–108.
- Kelley, C., Thompson, T.B., 1964. Tectonics and general geology of the Ruidoso-Carrizozo region, central New Mexico. New Mexico Geological Society Fall Field Conference Guidebook 15, 110–121.
- Knippertz, P., Stuut, J.-B.W. (Eds.), 2014. Mineral Dust. Springer, Netherlands, Dordrecht. Kocurek, G., Carr, M., Ewuing, R., Havholm, K.G., Nagar, Y.C., Singhvi, A.K., 2007. White Sands Dune Field, New Mexico: Age, dune dynamics and recent accumulations. Sedimentary Geology 197, 313–331.
- Konter, J.G., Storm, L.P., 2014. High precision 87Sr/86Sr measurements by MC-ICP-MS,

- simultaneously solving for Kr interferences and mass-based fractionation. Chemical Geology 385, 26–34.
- Kumar, A., Abouchami, W., Galer, S.J.G., Garrison, V.H., Williams, E., Andreae, M.O., 2014. A radiogenic isotope tracer study of transatlantic dust transport from Africa to the Caribbean. Atmospheric Environment 82, 130–143.
- Langford, R.P., 2003. The Holocene history of the White Sands dune field and influences on eolian deflation and playa lakes. Quaternary International 104, 31–39.
- Langford, R.P., Gill, T.E., Jones, S.B., 2016. Transport and mixing of eolian sand from local sources resulting in variations in grain size in a gypsum dune field, White Sands, New Mexico, USA. Sedimentary Geology 333, 184–197.
- Lawrence, C.R., Neff, J.C., 2009. The contemporary physical and chemical flux of aeolian dust: a synthesis of direct measurements of dust deposition. Chemical Geology 267, 46, 62
- Lawrence, C.R., Painter, T.H., Landry, C.C., Neff, J.C., 2010. Contemporary geochemical composition and flux of aeolian dust to the San Juan Mountains, Colorado, United States. Journal of Geophysical Research. https://doi.org/10.1029/2009JG001077.
- Lawrence, C.R., Reynolds, R.L., Ketterer, M.E., Neff, J.C., 2013. Aeolian controls of soil geochemistry and weathering fluxes in high-elevation ecosystems of the Rocky Mountains, Colorado. Geochimica et Cosmochimica Acta 107, 27–46.
- Lybrand, R.A., Rasmussen, C., 2018. Climate, topography, and dust influences on the mineral and geochemical evolution of granitic soils in southern Arizona. Geoderma 314, 245–261.
- Malm, W.C., Sisler, J.F., Huffman, D., Eldred, R.A., Cahill, T.A., 1994. Spatial and seasonal trends in particle concentration and optical extinction in the United States. Journal of Geophysical Research 99, 1347–1370.
- Marchand, D.E., 1970. Soil contamination in the White Mountains, eastern California. Geological Society of America Bulletin 81 (8), 2497–2506.
- Martin, W., 1964. Some aspects of the natural history of the Capitan and Jicarilla mountains and Sierra Blanca region of New Mexico. New Mexico Geological Society Fall Field Conference Guidebook 15, 171–176.
- Miller, O.L., Solomon, D.K., Fernandez, D.P., Cerling, T.E., Bowling, D.R., 2014.

 Evaluating the use of strontium isotopes in tree rings to record the isotopic signal of dust deposited on the Wasatch Mountains. Applied Geochemistry 50, 53–65.
- Muhs, D.R., Budahn, J.R., Prospero, J.M., Carey, S.N., 2007. Geochemical evidence for African dust inputs to soils of western Atlantic islands: Barbados, the Bahamas, and Florida. Journal of Geophysical Research-Earth Surface 112 (F2). https://doi.org/10. 1029/2005JF000445.
- Muhs, D., Budahn, J., Johnson, D., Reheis, M., Beann, J., Skipp, G., Fisher, E., Jones, J.A., 2008. Geochemical evidence for airborne dust additions to soils in Channel Islands National Park California. Geological Society of America Bulletin 120 (1–2), 106–126.
- Muhs, D.R., Budahn, J.R., Prospero, J.M., Skipp, G., Herwitz, S.R., 2012. Soil genesis on the island of Bermuda in the Quaternary: the importance of African dust transport and deposition. Journal of Geophysical Research 117, F03025. https://doi.org/10. 1029/2012.JF002366.
- National Trends Network, NADP: Precipitation data, accessible at http://nadp.sws.uiuc.edu/data/sites/siteDetails.aspx?net=NTN&id=NM08.
- Neff, J.C., Reynolds, R.L., Munson, S.M., Fernandez, D., Belnap, J., 2013. The role of dust storms in total atmospheric particle concentrations at two sites in the western US. Journal of Geophysical Research: Atmospheres 118 (19), 11201–11212.
- New Mexico Bureau of Geology and Mineral Resources, 2003. Geologic Map of New Mexico, Scale 1:500,000, accessible at https://geoinfo.nmt.edu/publications/maps/geologic/state/home.cfml.
- Nezat, C.A., Blum, J.D., Yanai, R.D., Hamburg, S.P., Park, B.B., 2008. Mineral sources of calcium and phosphorus in soils of the northeastern USA. Soil Science Society of America Journal 72 (6), 1786–1794.
- Pelt, E., Chabaux, F., Stille, P., Innocent, C., Ghaleb, B., Gérard, M., Guntzer, F., 2013. Atmospheric dust contribution to the budget of U-series nuclides in soils from the Mount Cameroon volcano. Chemical Geology 341, 147–157.
- Perez, A.E., Gill, T.E., 2009. Salt Flat Basin's contribution to regional dust production and potential influence on dry deposition in the Guadalupe Mountains (Texas, USA). Natural Resources and Environmental Issues 15, 117–118.
- Pett-Ridge, J.C., Derry, L.A., Barrows, J.K., 2009a. Ca/Sr and ⁸⁷Sr/⁸⁶Sr ratios as tracers of Ca and Sr cycling in the Rio Icacos watershed, Luquillo Mountains Puerto Rico. Chemical Geology 267 (1–2), 32–45.
- Pett-Ridge, J.C., Derry, L.A., Kurtz, A.C., 2009b. Sr isotopes as a tracer of weathering processes and dust inputs in a tropical granitoid watershed, Luquillo Mountains, Puerto Rico. Geochimica et Cosmochimica Acta 73, 25–43.
- Ponette-González, A.G., Collins, J.D., Manuel, J.E., Byers, T.A., Glass, G.A., Weathers, K.C., Gill, T.E., 2018. Wet dust deposition during the 2012 US drought: an overlooked pathway for elemental flux to ecosystems. Journal of Geophysical Research-Atmospheres. https://doi.org/10.1029/2018JD028806.
- Prospero, J.M., Ginoux, P., Torres, O., Nicholson, S.M., Gill, T.E., 2002. Environmental characterization of global sources of atmospheric soil dust identified with the NIMBUS 7 Total Ozone Mapping Spectrometer (TOMS) absorbing aerosol product. Reviews of Geophysics 40, 1002.
- Rasmussen, C., Brantley, S., Richter, D., Blum, A., Dixon, J., White, A.F., 2011. Strong climate and tectonic control on plagioclase weathering in granitic terrain. Earth and Planetary Science Letters 301, 521–530.
- Rawling, G.C., 2014. Geology of the Ruidoso Area, Lincoln and Otero Counties, New Mexico, New Mexico Bureau of Geology and Mineral Resources Open-File Report 507.
- Reheis, M., Kihl, R., 1995. Dust Deposition in southern Nevada and California, 1989, relations to climate, source area, and source lithology. Journal of Geophysical Research 100 (D5), 8893–8918.
- Reheis, M.C., Budahn, J.R., Lamothe, P.J., Reynolds, R.L., 2009. Compositions of modern dust and surface sediments in the Desert Southwest, United States. Journal of

- Geophysical Research 114, F01028.
- Reheis, M.C., Budahn, J.R., Lamothe, P.J., 2002. Geochemical evidence for diversity of dust sources in the southwestern United States. Geochimica et Cosmochimica Acta 66 (9), 1569–1587.
- Reynolds, R., Belnap, J., Reheis, M., Lamothe, P., Luiszer, F., 2001. Aeolian dust in Colorado Plateau soils: nutrient inputs and recent change in source. Proceedings of the National Academy of Sciences 98 (13), 7123–7127. https://doi.org/10.1073/ pnas.121094298.
- Reynolds, R., Neff, J., Reheis, M., Lamothe, P., 2006. Atmospheric dust in modern soil on aeolian sandstone, Colorado Plateau (USA): Variation with landscape position and contribution to potential plant nutrients. Geoderma 130 (1–2), 108–123.
- Rivas, J.A., 2019. Dust storms and the dispersal of aquatic invertebrates in the Chihuahuan Desert ecoregion. Ph.D. dissertation (Ecology and Evolutionary Biology), University of Texas at El Paso.
- Rivas Jr., J.A., Mohl, J.E., Van Pelt, R.S., Leung, M.Y., Wallace, R.L., Gill, T.E., Walsh, E.J., 2018. Evidence for regional aeolian transport of freshwater micrometazoans in arid regions. Limnology and Oceanography Letters 3 (4), 320–330.
- Rivas, J.A., Schröder, T., Gill, T.E., Wallace, R.L., Walsh, E.J., 2019. Anemochory of diapausing stages of microinvertebrates in North American drylands. Freshwater Biology 64 (7), 1303–1314. https://doi.org/10.1111/fwb.13306.
- Rivera Rivera, N.I., Gill, T.E., Bleiweiss, M.P., Hand, J.L., 2010. Source characteristics of hazardous Chihuahuan Desert dust outbreaks. Atmospheric Environment 44 (20), 2457–2468
- Sprankle, D.G., 1983. Soil Survey of Lincoln County Area. Department of Agriculture, Soil Conservation Service, New Mexico, US.
- Stone, E.L., Kalisz, P.J., 1991. On the maximum extent of tree roots. Forest Ecology and Management 46 (1–2), 59–102.

- Swap, R., Garstrang, M., Greco, S., Talbolt, R., Kallberg, P., 1992. Saharan dust in the Amazon Basin. Tellus 44B, 133–149.
- Szynkiewicz, A., Ewing, R.C., Moore, C.H., Glamoclija, M., Bustos, D., Pratt, L.M., 2010. Origin of terrestrial gypsum dunes—Implications for Martian gypsum-rich dunes of Olympia Undae. Geomorphology 121 (1–2), 69–83.
- Tchakerian, V., Pease, P., 2015. The critical zone in desert environments, developments in Earth surface processes. Elsevier 449–472.
- Trapp, J.M., Millero, F.J., Prospero, J.M., 2010. Temporal variability of the elemental composition of African dust measured in trade wind aerosols at Barbados and Miami. Marine Chemistry 120, 71–82.
- Vander Lee, B., Smith, R., Bate, J., 2004. Ecological and Biological Diversity of the Lincoln National Forest. In: Ecological and Biological Diversity of National Forests in Region 3, The Nature Conservancy.
- Van der Hoven, S.J., Quade, J., 2002. Tracing spatial and temporal variations in the sources of calcium in pedogenic carbonates in a semi-arid environment. Geoderma 108, 259–276.
- Vincent, J., Laurent, B., Losno, R., Bon Nguyen, E., Roullet, P., Sauvage, S., Chevaillier, S., Coddeville, P., Ouboulmane, N., di Sarra, A.G., Tovar-Sánchez, A., Sferlazzo, D., Massanet, A., Triquet, S., Morales Baquero, R., Fornier, M., Coursier, C., Desboeufs, K., Dulac, F., Bergametti, G., 2016. Variability of mineral dust deposition in the western Mediterranean basin and south-east of France. Atmospheric Chemistry and Physics 16, 8749–8766.
- Waterfall, U.T., 1946. Observations on the Desert Gypsum Flora of Southwestern Texas and Adjacent New Mexico. American Midland Naturalist 36 (2), 456–466.
- White, W.H., Hyslop, N.P., Trzepla, K., Yatkin, S., Rarig, R.S., Gill, T.E., Jin, L., 2015.
 Regional transport of a chemically distinctive dust: Gypsum from White Sands, New Mexico (USA). Aeolian Research 16, 1–10.